THE JOURNAL OF BIOLOGICAL CHEMISTRY VOL. 291, NO. 40, pp. 20946–20961, September 30, 2016

Structures of Exopolysaccharides Involved in Receptor-mediated Perception of *Mesorhizobium loti* by *Lotus japonicus*[*][S]

Received for publication, June 16, 2016, and in revised form, August 3, 2016 Published, JBC Papers in Press, August 8, 2016, DOI 10.1074/jbc.M116.743856

Artur Muszyński[‡1], Christian Heiss[‡], Christian T. Hjuler[§], John T. Sullivan[¶], Simon J. Kelly[¶2], Mikkel B. Thygesen[§], Jens Stougaard[‖], Parastoo Azadi[‡], Russell W. Carlson[‡], and Clive W. Ronson[¶3]

From the [‡]Complex Carbohydrate Research Center, University of Georgia, Athens, Georgia 30602, the [¶]Department of Microbiology and Immunology, University of Otago, Dunedin 9016, New Zealand, the [‖]Department of Molecular Biology and Genetics, Aarhus University, 8000 Aarhus C, Denmark, and the [§]Department of Chemistry, University of Copenhagen, 1871 Frederiksberg C, Denmark

In the symbiosis formed between *Mesorhizobium loti* strain R7A and *Lotus japonicus* Gifu, rhizobial exopolysaccharide (EPS) plays an important role in infection thread formation. Mutants of strain R7A affected in early exopolysaccharide biosynthetic steps form nitrogen-fixing nodules on *L. japonicus* Gifu after a delay, whereas mutants affected in mid or late biosynthetic steps induce uninfected nodule primordia. Recently, it was shown that a plant receptor-like kinase, EPR3, binds low molecular mass exopolysaccharide from strain R7A to regulate bacterial passage through the plant's epidermal cell layer (Kawaharada, Y., Kelly, S., Nielsen, M. W., Hjuler, C. T., Gysel, K., Muszyński, A., Carlson, R. W., Thygesen, M. B., Sandal, N., Asmussen, M. H., Vinther, M., Andersen, S. U., Krusell, L., Thirup, S., Jensen, K. J., *et al.* (2015) *Nature* 523, 308–312). In this work, we define the structure of both high and low molecular mass exopolysaccharide from R7A. The low molecular mass exopolysaccharide produced by R7A is a monomer unit of the acetylated octasaccharide with the structure (2,3/3-OAc)β-D-Rib*f*A-(1→4)-α-D-Glc*p*A-(1→4)-β-D-Glc*p*-(1→6)-(3OAc)β-D-Glc*p*-(1→6)-*[(2OAc)β-D-Glc*p*-(1→4)-(2/3OAc)β-D-Glc*p*-(1→4)-β-D-Glc*p*-(1→3)-β-D-Gal*p*]. We propose it is a biosynthetic constituent of high molecular mass EPS polymer. Every new repeating unit is attached via its reducing-end β-D-Gal*p* to C-4 of the fourth glucose (asterisked above) of the octasaccharide, forming a branch. The *O*-acetylation occurs on the four glycosyl residues in a non-stoichiometric ratio, and each octasaccharide subunit is on average substituted with three *O*-acetyl groups. The availability of these structures will facilitate studies of EPR3 receptor binding of symbiotically compatible and incompatible EPS and the positive or negative consequences on infection by the *M. loti exo* mutants synthesizing such EPS variants.

Rhizobia are soil bacteria that are able to form nitrogen-fixing endosymbiotic relationships with their host legume plants. In this mutualistic interaction, the host plant secretes flavonoids that stimulate compatible rhizobia to synthesize specific lipochitooligosaccharide signaling molecules called Nod factors (1, 2). The host plant perceives these Nod factors using membrane-bound receptor-like kinases that contain extracellular LysM domains (3–5). Perception of the Nod factors results in deformation and curling of root hairs and also the induction of cortical cell division to form nodule primordia (6). The bacteria entrapped in the curled root hairs form microcolonies and then enter the host through infection threads that are formed by localized digestion of the plant cell wall within the curl, followed by inverted growth of the cell wall/plasma membrane down the length of the root hair (7, 8). The rhizobia grow down the infection thread by cell division, and the infection thread ramifies as it reaches the growing nodule primordia. Eventually the rhizobia are released from the infection thread into the plant cell cytoplasm surrounded by a membrane of plant origin and develop into the nitrogen-fixing bacteroid form. The nodules formed may be either determinate (*e.g. Lotus* spp., *Phaseolus* spp., and *Glycine max*) or indeterminate (*e.g. Medicago* spp., *Vicia* spp., and *Trifolium* spp.) depending on the host (9). Determinate nodules have a short-lived meristem, and the nodules grow by plant cell expansion and division, resulting in nodules progressing through well defined developmental stages. In contrast, indeterminate nodules have a persistent meristem, and infection is continuous, resulting in all developmental stages being present within a single nodule.

Rhizobia produce a variety of cell surface-associated glycolipids and polysaccharides, as well as extracellular polysaccharides that also contribute to a successful symbiotic plant-

* This work was supported by Chemical Sciences Geosciences and Biosciences Division, Office of Basic Energy Sciences, United States Department of Energy Grant DE-FG02-93ER20097 to the Department of Energy-Center for Plant and Microbial Complex Carbohydrates at the Complex Carbohydrate Research Center (to A. M., C. H., R. W. C., and P. A.), and the Danish National Research Foundation Grant DNFR79 (to J. S.). The authors declare that they have no conflicts of interest with the contents of this article.

[S] This article contains supplemental Tables 1 and 2 and supplemental Figs. 1–6.

[1] To whom correspondence may be addressed: Complex Carbohydrate Research Center, University of Georgia, 315 Riverbend Rd., Athens, GA 30602. Tel.: 706-542-9496; Fax: 706-542-4412; E-mail: muszynski@ccrc.uga.edu.

[2] Present address: Dept. of Molecular Biology and Genetics, Aarhus University, 8000 Aarhus C, Denmark.

[3] To whom correspondence may be addressed: Dept. of Microbiology and Immunology, University of Otago, 720 Cumberland St., Dunedin 9016, New Zealand. Tel.: 64 3-479-7701; E-mail: Clive.Ronson@otago.ac.nz.

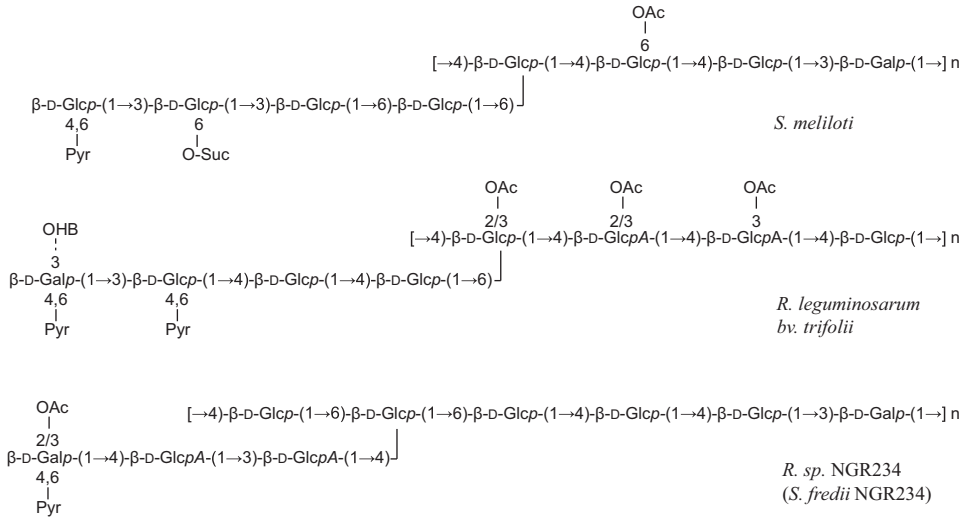

FIGURE 1. **Structures of exopolysaccharides from selected *Rhizobiales*: *S. meliloti* succinoglycan (EPS I) (16–20); *R. leguminosarum* (22–24); and *S. fredii* NGR234 (25).** "*2/3*", 3- or 2-linked; "*OHB*", hydroxybutanoate; "*Pyr*", pyruvate; "*OAc*", acetate; "*O-Suc*", succinate.

microbe interaction (10–15). Exopolysaccharides (EPS)[4] in particular are required for the formation and development of infection threads in indeterminate symbioses, of which the best characterized are those that occur between *Sinorhizobium meliloti* and *Medicago* species and between *Rhizobium leguminosarum* and *Vicia* species. Rhizobial EPS are usually branched or linear high molecular mass (HMM) heteropolymers or low molecular mass (LMM) oligomers composed of repeating units of 2–9 neutral or acidic sugar residues such as D-glucose, D-galactose, D-mannose, L-rhamnose, and D-glucuronic and D-galacturonic acids. Glycosyl residues are either β- or α-linked and may be substituted with *O*-succinyl, pyruvyl, *O*-acetyl, or *O*-methyl groups. The occurrence of these substitutions in the polymer is often regulated by environmental factors and may be either stoichiometric or non-stoichiometric. The uronic acids and some of the non-carbohydrate substituents provide acidic character and net negative charge to the EPS. The most extensively studied exopolysaccharide from *S. meliloti* strain 1021, succinoglycan, or EPS I, is a polymer consisting of an octasaccharide repeat unit composed of seven D-glucose and one D-galactose residues substituted with 6-*O*-succinyl, 6-*O*-acetyl, and 4,6-pyruvyl groups (Fig. 1). It is produced in both HMM and LMM (monomer, dimer, and trimer repeats of the octasaccharide) forms (16–20). Many *S. meliloti* strains but not strain 1021 also produce a second EPS, EPS II or galactoglucan, that consists of partially 6-*O*-acetylated D-glucose and 4,6-pyruvylated D-galactose disaccharide [β-D-Gal*p*-(1→3)-α-D-Glc*p*-(1→]$_n$ (21). Galactoglucan is able to replace the symbiotic requirement for succinoglycan in those strains that make it. In *R. leguminosarum*, the EPS polymer consists of a pyruvylated and *O*-acetylated octasaccharide repeat unit with a terminal non-reducing galactose residue (Fig. 1) (22–24). The role of EPS in symbiosis has also been extensively studied in the broad host range strain *Sinorhizobium fredii* NGR234, which produces a nonasaccharide EPS (Fig. 1) (25). The LMM forms of NGR234 EPS consist of the nonasaccharide monomer and an octasaccharide processed from it (26).

EPS may contribute to the establishment of the rhizobium-legume symbiosis in multiple ways, including physical roles such as mediating attachment, preventing agglutination, contributing to control of calcium ion fluxes, or providing protection against oxidative stress (27–31). However, studies of *S. meliloti* 1021 and *S. fredii* NGR234 have implicated EPS as playing a signaling role (20, 26, 28, 32–34). These studies suggested that succinoglycan trimers isolated from *S. meliloti* and the monomer oligosaccharides from *Rhizobium* sp. NGR234 were the symbiotically active species, as these species corrected the symbiotic defects of the EPS mutants when added exogenously (20, 26, 34). However, no plant receptors for the molecules were identified, and recent work has suggested that the *S. meliloti* LMM species are not required for symbiosis (35).

The genetics and biochemistry of succinoglycan biosynthesis in *S. meliloti* 1021 have been extensively characterized, and most biosynthetic genes except one required to add the terminal glucose to the branch have been identified (13, 36). Mutations that abolish synthesis and some that modify succinoglycan structure cause symbiotic defects. For example, mutants in *exoY*, which initiates the first step in succinoglycan biosynthesis, still develop infection foci in curled root hairs but rarely initiate formation of infection threads. HMM succinoglycan is cleaved by two glycanases ExsH and ExoK (37), to produce a pool of monomers, dimers, and trimers of the octasaccharide repeat unit.

Recently, rhizobial EPS has also been shown to play a role in infection thread formation in determinate symbioses. *Mesorhizobium loti* strain R7A mutants affected in different stages of the EPS biosynthesis pathway exhibit different symbiotic phe-

[4] The abbreviations used are: EPS, exopolysaccharide; COSY, homonuclear correlation spectroscopy; HMBC, heteronuclear multiple-bond correlation spectroscopy; HMM, high molecular mass (high molecular weight); HSQC, heteronuclear single-quantum correlation spectroscopy; LMM, low molecular mass (low molecular weight); PMAA, partially methylated alditol acetate; ROESY, rotating frame nuclear Overhauser effect spectroscopy; TOCSY, total correlation spectroscopy; XR ESI/MALDI-FT-ICR-MS, eXtreme resolution electrospray ionization/matrix assisted laser desorption time of flight-Fourier transform-ion cyclotron resonance mass spectrometry; 1D, one-dimensional; 2D, two-dimensional.

notypes on the model legume *Lotus japonicus* Gifu depending on the step at which EPS biosynthesis is halted. Mutants in genes affecting synthesis of the EPS backbone (*exoB* and *exoA*) form nitrogen-fixing nodules but with a delay compared with wild-type R7A (38). In contrast, mutants involved in synthesis of the EPS branch (*e.g. exoU* and *exoO*) form infection foci within curled root hairs, but only a few short infection threads are observed, and these fail to extend (38, 40). Several lines of evidence suggest that *M. loti* EPS acts as a positive signaling molecule. A Tn*5* transposon mutant with an insertion within the 3′ end of *exoU* had a similar dry-colony morphology to a null *exoU* mutant, but compositional analysis revealed it produced a small quantity of wild-type EPS. This mutant nodulated *L. japonicus* normally. *In vivo* complementation experiments performed using mixtures of the *exoU* mutant and a *nodA* mutant strain, which produced wild-type EPS but was unable to form nodules, showed that EPS allowed infection thread extension to the base of root hairs but not through to the cortical cell layer (38).

A search for plant mutants able to form nodules with the *M. loti exoU* mutant led to the identification of a specific *L. japonicus* receptor EPR3 that directly perceives *M. loti* EPS. EPR3 is a membrane-bound receptor-like kinase containing three LysM domains within the amino-terminal region. It was proposed that it differentiates between compatible and incompatible forms of EPS to regulate the passage of the beneficial bacteria through the plant's epidermal cell layer (40). An octasaccharide component of *M. loti* strain R7A EPS bound directly to the purified ecto-domain of EPR3 in *in vitro* binding assays, thus confirming the signaling role of LMM EPS in symbiosis.

These studies and future studies of receptor-ligand binding require the determination of the structure of both HMM and LMM EPS from *M. loti* strain R7A. In this study, we report the determination of the structure of both the HMM and LMM EPS from *M. loti* R7A, including the location of the four non-stoichiometric *O*-acetyl substituents.

Results

We have previously reported that GC/MS composition analysis of R7A EPS showed the presence of Glc, Gal, Glc*p*A, and Rib*f*A (38). The stereochemical configurations of Glc, Gal, GlcA, and RibA (carboxyl reduced to Rib) were all assigned as "D" based on comparison of the retention times of their trimethylsilyl-(*S*)-(+)-2-butyl glycosides with the authentic standards of D-Glc, D-Gal, D-GlcA, and D-Rib. Below, we determine the structures of both HMM and LMM EPS from R7A.

Glycosyl Linkage Analyses of HMM EPS—Glycosyl linkage determination was performed by methylation analysis of PMAA derivatives before and after reduction of carboxyl groups with sodium borodeuteride. Before reduction, GC/MS analysis of the PMAAs showed the presence of 3-linked Gal*p*, 4,6-linked Glc*p*, 6-linked Glc*p*, and 4-linked Glc*p* in a 1.0:0.93:1.1:3.3 ratio. To identify the Glc*p*A and Rib*f*A linkages, methylation analysis was also performed after carboxyl group reduction (supplemental Fig. 1). In the case of GlcA, carboxyl reduction resulted in its conversion to a 4-linked Glc-6-D_2 residue as indicated by the presence of primary fragment ions of *m*/*z* 118 and *m*/*z* 235 in its PMAA derivative. The PMAA of 4-linked Glc*p* normally gives ions of *m*/*z* 118 and 233, which were also observed; however, after carboxyl reduction, the appearance of the *m*/*z* 235 ion provided proof of a 4-linked Glc residue that was derived from 4-linked Glc*p*A due to the two deuterium atoms present at C6 (supplemental Fig. 1*A*). A small amount of terminal Glc*p*A (characterized by primary fragment ions of *m*/*z* 163 and 207) was also observed (supplemental Fig. 1*B*). The Rib*f*A was converted to Rib*f*-$5D_2$ with two deuterium atoms at C5. The GC/MS analysis showed that its PMAA derivative was consistent with it being present as a terminal residue (supplemental Fig. 1*C*). Thus, this EPS consists of 3-linked Gal*p*, 4,6-linked Glc*p*, 6-linked Glc*p*, and 4-linked Glc*p* and 4-linked Glc*p*A in an approximate 1:1:1:3:1 ratio and with terminal Rib*f*A suggesting a polymer built of eight glycosyl residues (residues A–H).

NMR Analysis of Glycosyl Sequence in HMM EPS—Initial proton NMR analysis of HMM EPS showed poor spectral resolution due to extreme viscosity but indicated extensive *O*-acetylation of the polymer (supplemental Fig. 2). The location of *O*-acetyl groups on the *M. loti* R7A EPS is discussed further below. However, to simplify the EPS glycosyl residue structural analysis, the sample was de-*O*-acetylated prior to NMR analysis, which significantly improved the quality of the spectra. The anomeric signals of the Rib*f*A (residue A) and Glc*p*A (residue B) resonated at 4.96 and 5.27 ppm, respectively (Table 1 and Fig. 2). Following the connectivities and measuring chemical shift values in the COSY, TOCSY, and HSQC spectra yielded the complete chemical shift assignments of these two residues. The carbon chemical shifts of the Rib*f*A residue were consistent with reported values for an unsubstituted β-anomer (41). The β-configuration was also supported by the J_{1-2} coupling constant of less than 2 Hz; the reported values for α- and β-anomers of Rib*f*A are 4.1 and 1.7 Hz, respectively (41). The chemical shifts for H1/C1 of GlcA*p* $(B)_{H1/C1}$ of 5.27/100.4 ppm point to an α-anomer, and the downfield carbon shift for C4 at 82.4 ppm (B4) is indicative of glycosylation at this position, a result that is consistent with the methylation data demonstrating a 4-linked GlcA residue (supplemental Fig. 1*A*). The HMBC spectrum demonstrated that the Rib*f*A residue was linked to the 4-position of the Glc*p*A residue by showing a cross-peak between the Rib*f*A H1 at 4.96 ppm and the C4 of Glc*p*A at 82.4 ppm (A_{H1}/B_{C4}, Fig. 3*A*) and also coupling between the C1 of Rib*f*A and H4 of Glc*p*A (109.7/3.49 ppm) (A_{C1}/B_{H4}, Fig. 3*B*). The NOE cross-peak at 5.27/3.55 ppm (B_{H1}/Glc_{H4}) (Fig. 3*C*) showed a close contact between H1 of GlcA*p* and H4 of a Glc*p* residue, providing proof of a 1→4 linkage between Glc*p*A and Glc*p*. This linkage was also supported by the HMBC experiment, which showed Glc*p*A C1 to Glc*p* H4 coupling at 100.4/3.55 ppm (B_{C1}/Glc_{H4}) (Fig. 3*B*). Thus, these data support the following terminal trisaccharide glycosyl sequence as being a part of the oligosaccharide branch of the EPS repeat unit structure: β-D-Rib*f*A-(1→4)-α-D-Glc*p*A-(1→4)-D-Glc*p*-(1→ (trisaccharide unit A-B-C). Additionally, the methylation data, which showed that a small portion of Glc*p*A was present as a terminal linkage (supplemental Fig. 1*A*), suggested that Rib*f*A is occasionally absent, resulting in terminal α-D-Glc*p*A-(1→4)-β-D-Glc*p*-(1→ disaccharide sequence. Indeed, we were able to

TABLE 1
The ^{1}H and ^{13}C chemical shift assignments for the HMM *M. loti* R7A EPS

Residue	H1 C1	H2 C2	H3 C3	H4 C4	H5 C5	H6a/b C6
A, β-Rib*f*	4.96	4.01	4.34	4.21		
	109.7	75.2	74.7	82.9		
B, 4-β-GlcA	5.27	3.64	3.71	3.49	3.95	
	100.4	71.8	71.9	82.4	73.2	
Bt,[a] t-β-GlcA	5.31	3.58	3.72	3.49	3.95	
	100.4	72.0	72.0	72.3	73.3	
D, 6-β-Glc	4.47–4.49[i]	3.30–3.39[i]	3.47	3.45	3.56–3.65[i]	4.16/3.84
	103.3	73.5	76.1	70.2	74.7–75.4	69.2
E, 4,6-β-Glc	4.50	3.30	3.68	3.72	3.76	4.23/3.90
	103.3	73.6	75.3	78.9	74.2	68.9
C,F,G, 4-β-Glc	4.47–4.49[b]	3.30–3.39[b]	3.56–3.65[b]	3.55−3.64[b]	3.56–3.65[b]	3.93–3.89/3.79–3.73[b]
	103.3	73.5	74.7–75.4	78.5–79.3	74.7–75.4	60.8–61.3
H, β-Gal	4.49	3.68	3.76	4.13	3.76	ND[c]
	103.3	70.7	82.8	68.9	74.2	

[a] Bt indicates terminal residue B.
[b] Because of the overlapping resonances, it is not possible to identify which resonances belong to which Glc residue.
[c] ND means not detected.

observe weak NMR signals of a spin system due to the terminal Glc*p*A residue with the H1/C1 at 5.31/100.4 ppm (residue Bt) (Table 1 and Fig. 2).

The remaining anomeric signals in the spectra of HMM EPS were extensively overlapped so that a complete assignment for these residues was not possible. Most of these signals resonated near 4.5 ppm and formed a cluster corresponding to five protons. A signal at 4.49/4.13 ppm in the TOCSY suggested that one of the anomeric protons in this cluster belonged to a β-Gal residue (residue H). Its assignment, including chemical shifts of H1/C1 through H5/C5, was possible by using the chemical shift prediction calculation CASPER tool (42) (supplemental Table 1). The remainder of the group of signals around 4.5 ppm were therefore from β-Glc residues. The anomeric β-configuration was assigned by comparison of carbon and proton chemical shifts with common literature values. Some overlapping peaks near 4.6 ppm were also characterized as belonging to β-Glc by the upfield chemical shift of their H2 protons (3.30–3.40 ppm). The COSY and TOCSY spectra (Fig. 2*B* and supplemental Fig. 3), together with the HSQC spectrum (Fig. 2*A*), showed that two Glc*p* ring systems had H6/C6 resonances at 4.16–3.90/68.9–69.2 ppm (see Table 1); the downfield chemical shifts for C6 supported the assignment of these resonances to the two Glc*p* residues that are substituted at C6, *i.e.* the 6- and 4,6-linked Glc*p* residues (residues D and E, respectively). The H6/C1 coupling at 3.83/103.3 ppm in the HMBC spectrum (Fig. 3*B* (Hex_{C1}/Glc_{H6})) supported β-Hex-(1→6)-β-Glc and/or β-Hex-(1→6)-[β-Hex-(1→4)-]β-Glc*p* sequences, consistent with the methylation data, which showed 6- and 4,6-linked Glc*p* residues. The ^{1}H and ^{13}C chemical shift assignments for HMM EPS are summarized in Table 1.

Because of the extensive overlap of the anomeric signals of the various Glc*p* residues, no further definite structural information was available from the spectra of HMM EPS. Therefore, we concentrated our efforts on the structural characterization of LMM EPS.

Determination of Glycosyl Sequence of De-O-acetylated LMM EPS—To determine the monosaccharide sequence of EPS, we attempted analysis of LMM EPS from *M. loti* R7A. Co-extraction and co-precipitation of associated cyclic β-glucan along with EPS (38) made the analysis difficult. We took advantage of the availability of an *M. loti* R7A *ndvB* mutant that produces both HMM and LMM EPS but is unable to synthesize cyclic β-glucans (38). The size exclusion chromatography elution profile of crude LMM R7A*ndvB* EPS indicated the presence of only one major fraction that eluted slightly ahead of the standard of maltoheptaose (supplemental Fig. 4), suggesting that LMM EPS was represented by only one type of oligosaccharide of homogeneous size. This was confirmed by MALDI-TOF MS displaying a molecular ion corresponding to $RibAGlcAHex_6OAc_3$ (Fig. 6*B*). Initial comparative NMR analysis of HMM and LMM exopolysaccharides from both R7A and R7A*ndvB* indicated their structural similarity (see also MALDI MS analysis of *O*-acetylated LMM EPS below). The PMAA linkage analysis with methylation done after carboxyl reduction indicated the presence of 6-linked Glc*p*, 4-linked Glc*p*, terminal Rib*f*A, and 4-linked Glc*p*A in an approximate ratio of 2:3:1:1, with some terminal Glc*p*A and traces of a 3-linked Gal*p* residue. The latter was detected in a smaller quantity and underwent partial degradation and modification in that it was converted to its furanose form, and in addition, the C1 of Gal was partially converted to a methyl glycoside during carboxyl esterification by methanolysis. As a result, we observed an early eluting peak in GC/MS due to Gal with a diagnostic electron ionization fragment at *m*/*z* 206 (supplemental Fig. 1*D*). These findings suggest that the galactose residue was at the reducing end of the LMM EPS. Unlike the HMM R7A polymer, no PMAA corresponding to the branching 4,6-linked Glc*p* was found in the LMM EPS, suggesting it could be an attachment point for a new subunit of the polymer. This result indicates that the LMM EPS is likely a single repeat unit of EPS.

These initial PMAA composition data on *ndvB* LMM EPS were supported by 1D and 2D NMR analyses on de-*O*-acetylated EPS. The 1D proton spectrum showed the same general signal pattern as that of de-*O*-acetylated HMM EPS but was of much better quality and higher resolution as a result of the small molecular weight of LMM EPS. As in the case of de-*O*-acetylated HMM EPS, β-Rib*f*A and α-Glc*p*A were easily identified, and their chemical shifts were assigned from the COSY, TOCSY, and HSQC spectra. Likewise, the inter-residue connections between O-1 of Rib*f*A and O-4 of Glc*p*A, as well as that from O-1 of Glc*p*A to O-4 of a β-Glc residue (trisaccharide unit

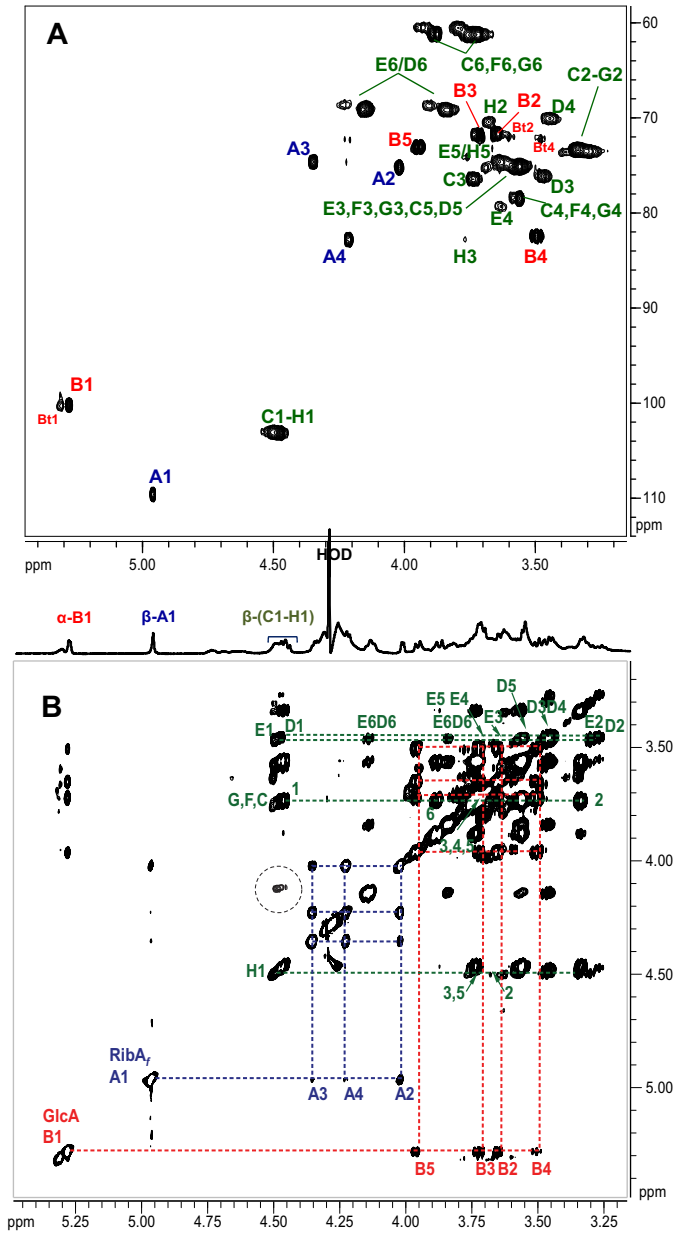

FIGURE 2. **HSQC (*A*) and TOCSY (*B*) spectrum of the de-*O*-acetylated HMM EPS from *M. loti* R7A.** The glycosyl residues A–H are as indicated in Table 2. All spectra were recorded at 70 °C. *Dotted circle* in *B* highlights an H4 residue of 3-β-Gal*p*. This low intensity signal was locally increased and does not represent actual abundance in comparison with intensities of chemical shifts of the remaining residues.

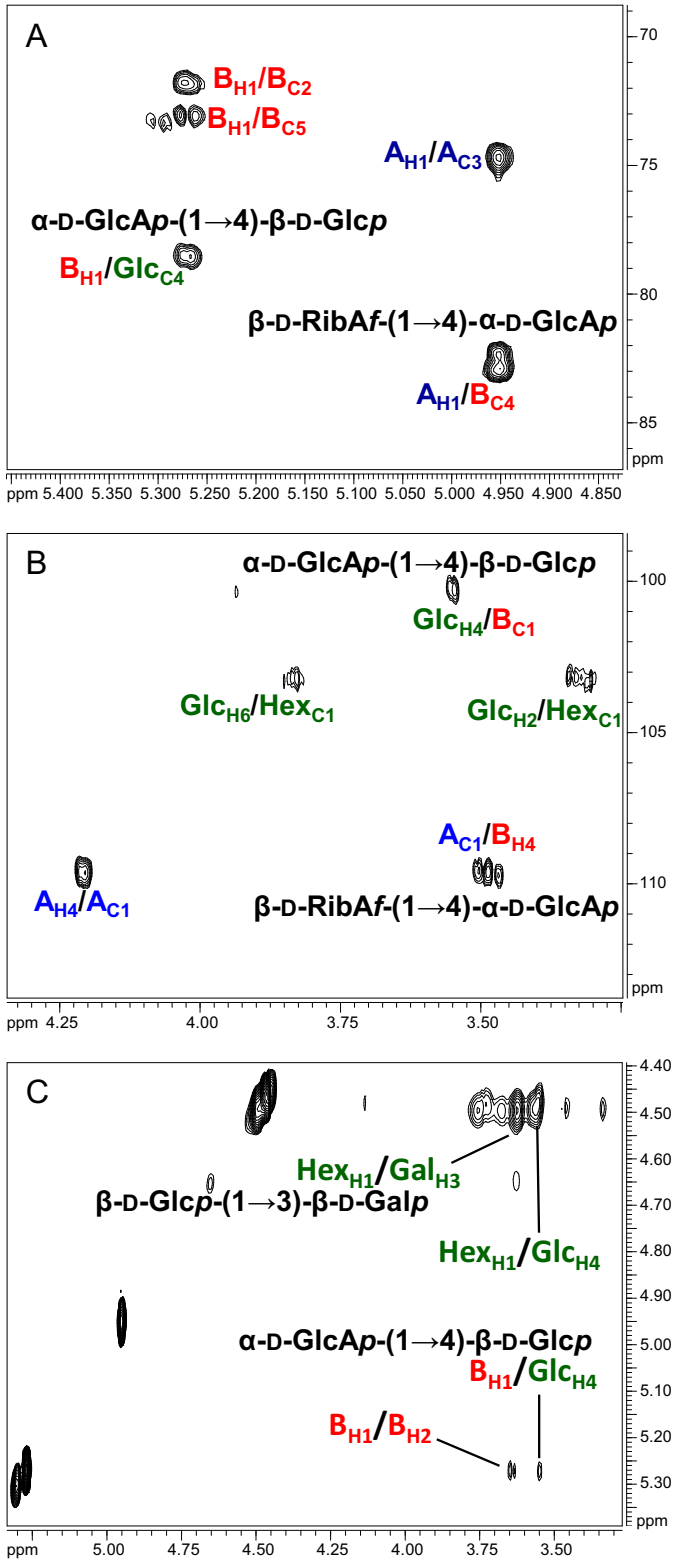

FIGURE 3. **Anomeric regions of the HMBC (*A* and *B*) and NOESY (*C*) spectra of the de-*O*-acetylated HMM EPS from *M. loti* R7A.** The glycosyl residues A–H are as indicated in Table 2. All spectra were recorded at 70 °C. *Hex,* gluco or galactosyl residue.

A-B-C), were confirmed by correlations in both ROESY and HMBC spectra (Fig. 4 and Table 2). However, in contrast to the spectra of HMM EPS, TOCSY and ROESY of LMM EPS were able to resolve the four β-Glc*p* spin systems whose anomeric proton resonances clustered around 4.5 ppm, such that a complete assignment of these residues became possible. Two of these were found to be 4-linked β-Glc*p*, and the other two were 6-linked β-Glc*p* residues. In addition to these residues, there was a set of two almost identical spin systems with chemical shifts consistent with 4-linked β-Glc*p*. Their anomeric proton signals resonated at 4.7 ppm with a combined integral of one proton, suggesting that these spin systems corresponded to two variants of the same 4-linked β-Glc*p* residue in the oligosaccharide. Finally, there were two variants of the 3-linked Gal*p* residue, one α- and one β-anomeric configuration (residues Hα and Hβ, respectively). Both of these 3-linked Gal*p* variants had upfield chemical shifts of their anomeric carbons (92.6 and 96.6

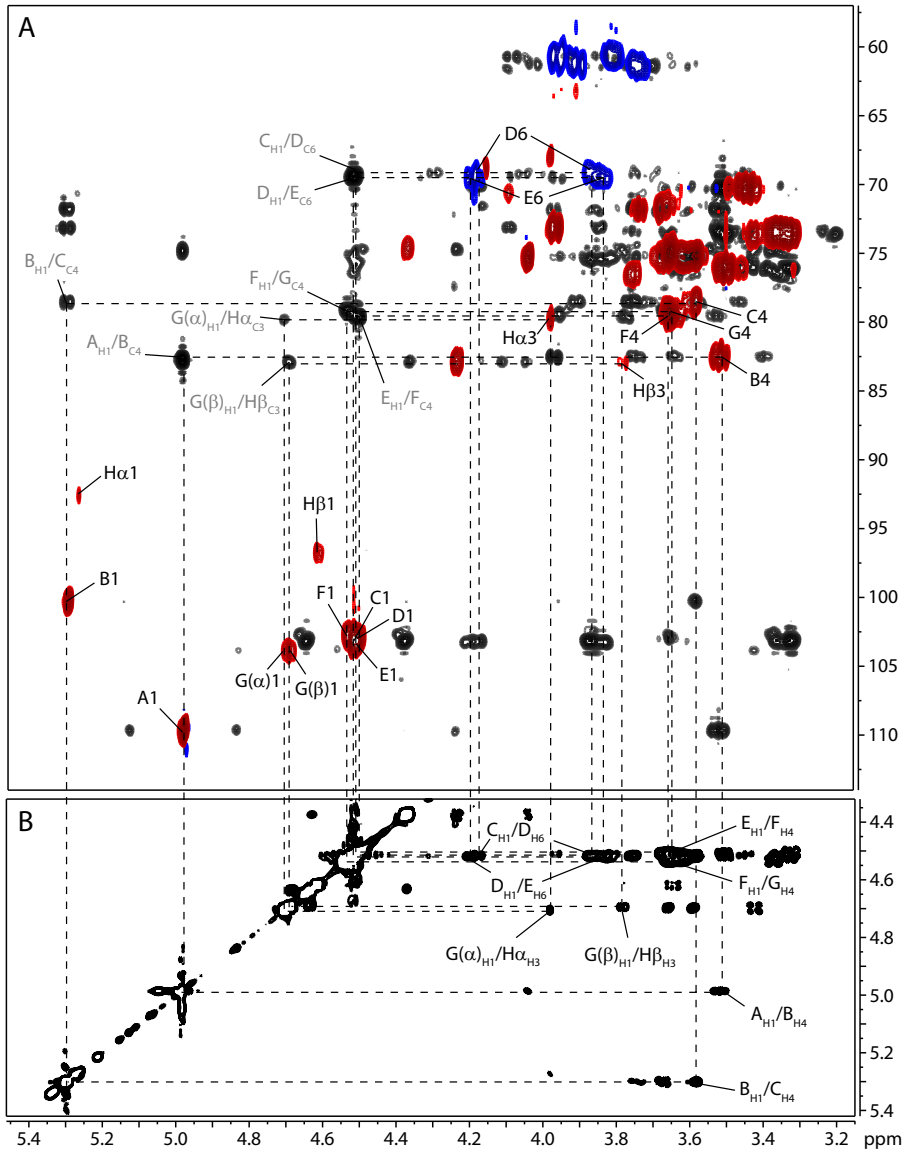

FIGURE 4. **NMR spectroscopy of de-*O*-acetylated R7A*ndvB* octasaccharide.** *A*, overlaid multiplicity-edited ^{1}H-^{13}C HSQC (CH_3 and CH signals have positive phase and are drawn in *red*; CH_2 signals have negative phase and are drawn in *blue*) and HMBC (*black*) spectra; *B*, lower section of the anomeric region of the ^{1}H-^{1}H-ROESY spectrum. *Peaks* that indicate the sequence of the oligosaccharide are labeled. All spectra were recorded at 70 °C.

ppm, respectively, see Table 2) identifying them as the two anomeric forms of the reducing end residue of the LMM oligosaccharide. ROESY and HMBC spectra were used to define the remainder of the monosaccharide sequence (Fig. 4 and Table 2). Unambiguous ROESY and HMBC correlations were found between H3 of 3-β-Gal*p* (residue Hβ) and one of the two 4-β-Glc*p* anomeric signals near 4.7 ppm (residue G(β)), as well as between H3 of 3-α-Gal*p* (residue Hα) and H1 of the other 4-β-Glc*p* (residue G(α)). At the other end of the sequence, the 4-linked β-Glc*p* (residue C) that is proximal to the 4-β-Glc*p*A residue was identified by ROESY and HMBC correlations with H1 of GlcA pinpointing the H4/C4 chemical shifts of that residue to 3.59/78.4 ppm. TOCSY and HSQC showed that this signal is part of the spin system whose H1 resonated at 4.512 ppm. H1 of residue C in turn showed ROESY correlations with signals at 4.18 and 3.86 ppm, which arose from H6a and H6b of residue D, demonstrating the linkage of residue C to O-6 of residue D. The ROESY cross-peaks of the anomeric signal of residue D matched with the H6 resonances associated in the TOCSY spectrum with residue E. The anomeric signal of the latter exhibited a ROESY cross-peak at 3.66 ppm, which coincided with H4 of both residues F and G. However, the linkage from residue E to residue F was clearly evidenced by an HMBC correlation of H1 of residue E to a signal at 79.3 ppm, belonging to C-4 of residue F.

This last connection completed the sequence analysis of the de-*O*-acetylated oligosaccharide, and we determined its structure as the β-Rib*f*A-(1→4)-α-Glc*p*A-(1→4)-β-Glc*p*-(1→6)-β-Glc*p*-(1→6)-β-Glc*p*-(1→4)-β-Glc*p*-(1→4)-β-Glc*p*-(1→3)-Gal*p* octasaccharide.

LMM Octasaccharide Is a Constituent of HMM EPS Polymer—Composition and linkage analysis of glycosyl residues combined with NMR studies performed on de-*O*-acetylated HMM and LMM EPS demonstrated that the repeating unit of HMM

TABLE 2

Proton ^{1}H and carbon ^{13}C chemical shift assignments of de-*O*-acetylated R7A*ndvB* LMM oligosaccharide

Residues marked in bold are main residues.

Residue		H1 C1	H2 C2	H3 C3	H4 C4	H5 C5	H6a C6	H6b
A	β-Rib*f*A-(1→4)	4.98	4.04	4.37	4.24			
		109.6	75.3	74.6	82.8	179		
B	4-α-Glc*p*A-(1→4)	5.30	3.67	3.74	3.52	3.97		
		100.3	71.6	71.8	82.4	73.0	175.3	
C	4-β-Glc*p*-(1→6)	4.512	3.354	3.75	3.59	3.58	3.90	3.75
		102.9	73.5	76.5	78.4	75.2	61.2	
D	6-β-Glc*p*-(1→6)	4.516	3.329	3.51	3.45	3.61	4.18	3.86
		103.0	73.4	76.0	70.1	75.2	69.5	
E	6-β-Glc*p*-(1→6)	4.502	3.32	3.51	3.44	3.68	4.20	3.83
		103	73.4	76.0	70.1	75.3	69.5	
F	4-β-Glc*p*-(1→4)	4.533	3.368	3.65	3.66	3.62	3.96	3.8
		102.9	73.4	74.8	79.3	75.3	60.6	
G (α)[a]	4-β-Glc*p*-(1→4)	4.706	3.409	3.662	3.66	3.58	3.94	3.81
		103.9	73.8	74.7	78.6	75.2	60.6	
G (β)[a]	4-β-Glc*p*-(1→4)	4.693	3.443	3.655	3.66	3.58	3.94	3.81
		103.9	73.8	74.7	78.6	75.2	60.6	
Hα	3-α-Gal*p*	5.28	3.98	3.98	4.22	4.09	3.72	3.72
		92.6	68.0	79.8	69.9	70.6	61.4	
Hβ	3-β-Gal*p*	4.62	3.64	3.78	4.16	3.70	ND[b]	ND
		96.6	71.1	82.8	68.7	75.4	ND	

[a] Symbols in parentheses refer to the anomeric configuration of residue H (galactose at the reducing end present as an α- or β-anomer).
[b] ND means not detected.

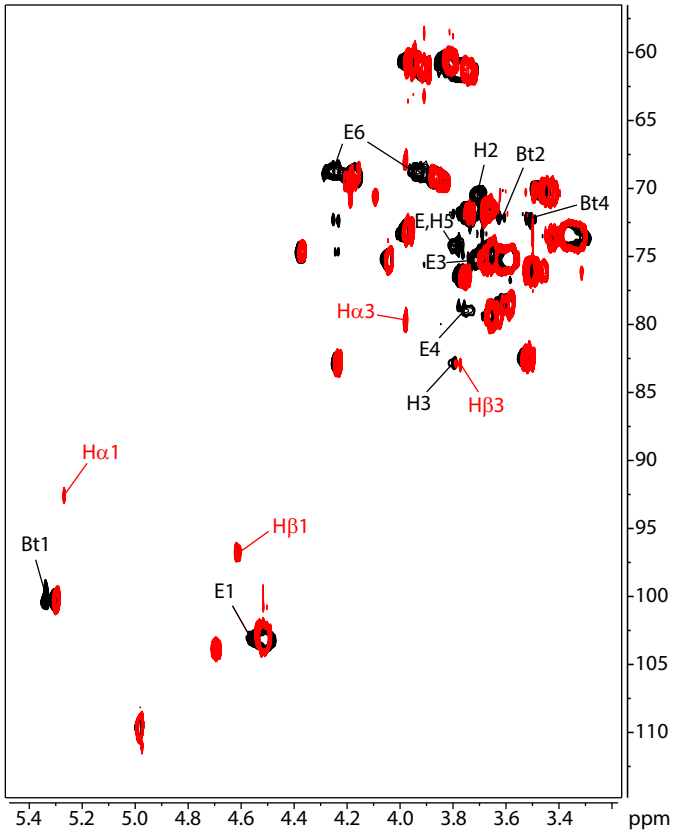

FIGURE 5. **Overlaid ^{1}H-^{13}C HSQC NMR spectra of de-*O*-acetylated HMM (*black*) and LMM (*red*) EPS, confirming the hypothesis that the octasaccharide is the monomeric repeating unit of HMM EPS.** The only signals that are different in both spectra are those belonging to the residues involved in connecting the subunits to each other (residues E and H) and those belonging to terminal GlcA (residue *Bt*), which is substoichiometric in HMM EPS but stoichiometric in LMM EPS. The chemical shift changes observed in residues E and H upon polymerization are consistent with predicted values as described previously (42).

EPS was almost identical to the octasaccharide, except that residue E was 4,6-β-linked in the polymer and 6-β-linked in the octasaccharide (refer to previous sections). This indicated that residue E contained both the possible branching and polymerization sites in HMM EPS. Therefore, we hypothesized that the LMM octasaccharide would be a subunit of the HMM EPS. If this was the case, the NMR chemical shifts of the different spin systems of LMM and HMM EPS should be the same, except for those involved in the branch point, *i.e.* residues E (Glc*p*) and H (Gal*p*). To test this hypothesis, we overlaid and compared the ^{1}H-^{13}C HSQC spectra of the de-*O*-acetylated HMM and LMM and identified the signals that were unique in each spectrum (Fig. 5, *red,* LMM octasaccharide; *black,* HMM polymer). The two spectra were almost identical with few exceptions, which were accounted for by the different polymerization states of the two saccharides. Most of the signals unique to HMM EPS belonged to a 4,6-linked Glc*p* (residue E). These signals were shifted downfield in the proton dimension relative to the corresponding 6-linked Glc*p* residue in LMM EPS. These differences in proton, as well as in the carbon, chemical shifts of residue E in the two saccharides are in excellent agreement with what is predicted by the CASPER chemical shift calculation tool (42) (see supplemental Table 1). The replacement of a 6-linked Glc by a 4,6-linked Glc is accounted for by the polymerization of the octasaccharide, which forms a bond between O-4 of residue E and O-1 of residue H. Involvement of the latter residue in the polymerization was confirmed by the presence of two HSQC signals appearing only in the spectrum of HMM, namely those of H2 and H5 of β-Gal. Conversely, upfield anomeric carbon chemical shifts of α-Gal and β-Gal, as well as H3 of α-Gal appeared only in the spectrum of the octasaccharide where the Gal residue, being located at the reducing end, is able to undergo mutarotation, giving rise to both α- and β-anomers. The final difference observed in the two spectra was the presence of terminal GlcA only in the spectrum of HMM EPS. As already shown by the linkage data, some repeating units in the polymer lack the riburonic acid residue, whereas the GlcA in LMM EPS is stoichiometrically substituted with Rib*f*A.

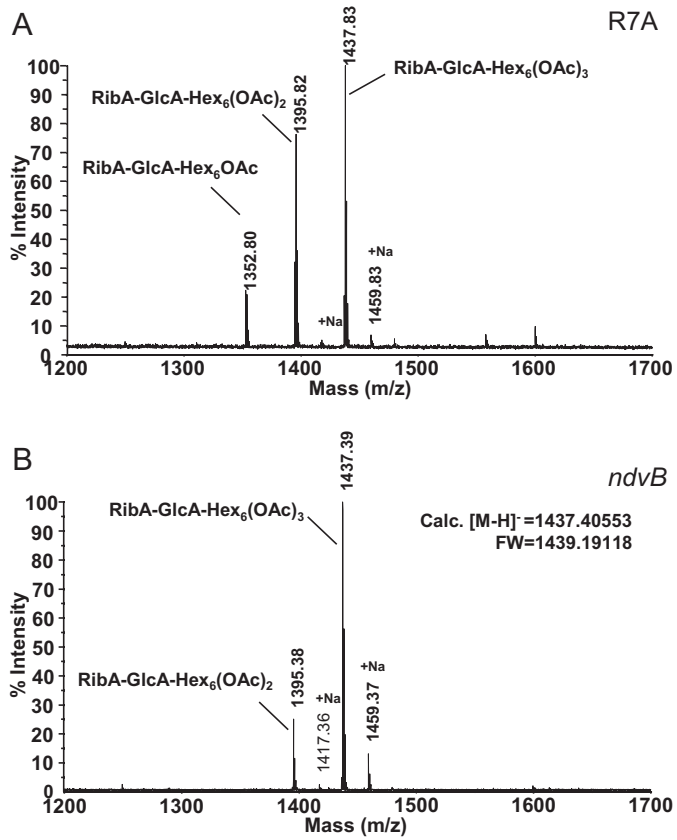

FIGURE 6. **MALDI-TOF MS analysis of LMM EPS isolated from *M. loti* R7A (*A*) and its *ndvB* mutant (*B*).** The spectra were acquired in the negative reflectron-mode and show monoisotopic $[M - H]^-$ ions.

Taken together, these data provide strong evidence that the octasaccharide derives from the polymer and is the repeating unit of HMM EPS. In addition, this analysis complements and provides missing information for residues E and H in the polymer (Table 1).

Localization of O-Acetyl Groups in the LMM Monomeric Octasaccharide Unit of EPS—Comparison of the MALDI-TOF MS analysis of the wild-type R7A LMM EPS (Fig. 6*A*) with the LMM EPS of R7A*ndvB* (Fig. 6*B*) showed that both have the same molecular ions and that these LMM EPS are *O*-acetylated octasaccharides with one, two, or three *O*-acetyl groups. Analysis of the LMM EPS from R7A showed the presence of three monoisotopic $[M - H]^-$ signals at *m*/*z* 1437.83, 1395.82, and 1352.80, respectively. The 42-Da mass differences indicated varying *O*-acetyl substitutions, and the masses were consistent with a $RibAGlcAHex_6$ octasaccharide substituted with three, two, or one *O*-acetyl groups, respectively. Similarly, analysis of the LMM EPS from the R7A *ndvB* mutant showed ions of 1437.39 and 1395.38 consistent with the same octasaccharide with three and two *O*-acetyl groups, respectively. These data, together with the structural analysis described above, support the conclusion that the LMM EPS from both R7A and its *ndvB* mutant is an octasaccharide, representing one repeat unit of the EPS polymer $(RibAGlcAGlc_5Gal)_n$ substituted with one to three *O*-acetyl groups.

A series of NMR experiments on *O*-acetylated R7AndvB LMM EPS supported the presence of eight glycosyl residues (A–H), consistent with NMR analysis of the de-*O*-acetylated LMM EPS described above. To streamline data interpretation, we marked the position of the *O*-acetyl substituent(s) on the glycosyl residue with a subscripted number, *e.g.* A_3 and $A_{2,3}$ for 3-*O*-acetylated and 2,3-di-*O*-acetylated residue A, respectively. Different NMR variants of the same glycosyl residue, likely due to different substitution patterns by *O*-acetyl groups on neighboring residues, were labeled with prime marks, *e.g.* E′, E″, E‴, respectively. The 2D TOCSY spectrum showed nearly 30 individual monosaccharide residues (Fig. 7*A*). Tracing connectivities in the COSY spectrum and reading the corresponding carbon chemical shifts from the HSQC spectrum allowed us to assign chemical shifts to most of the protons and carbons of 23 of these residues (Table 3). Downfield carbon chemical shift displacements relative to the corresponding monomeric sugars were used to identify glycosylated positions and allowed us to classify the linkage type of each residue. The anomeric configuration of each residue was determined by $J_{1,2}$ proton-proton coupling constants and comparison of carbon and proton chemical shifts with common literature values. Thus, we found three terminal β-Rib*f*A residues (A, $A_{2,3}$, and A_3), one 4-β-Glc*p*A residue (B), seven 4-β-Glc*p* residues (C, C′, G, G′, F_2, F_3, and F_3'), 10 6-β-Glc*p* residues (D, D_3, D_3', D_3'', E, E′, E″, E‴, E_2, and E_2'), and the α- and β-forms of the reducing-end Gal*p* residue (Hα and Hβ, respectively) (Table 3). Downfield proton chemical shift displacements were indicative of *O*-acetylation. The three β-Rib*f*A residues were distinguished by their acetylation patterns in that $A_{2,3}$ was 2,3-di-*O*-acetylated, A_3 was 3-*O*-acetylated, and A was not acetylated. One of the 4-β-Glc*p* residues was 2-*O*-acetylated (F_2), two were 3-*O*-acetylated (F_3 and F_3'), and four were not acetylated (C, C′, G, and G′). Three of the 6-β-Glc*p* residues were 3-*O*-acetylated (D_3, D_3', and D_3''), two were 2-*O*-acetylated (E_2 and E_2'), and five were not acetylated (D, E, E′, E″, and E‴). Residues G and G′ were identified as adjacent to the reducing end of Gal (H) due to cross-peaks to a resonance at 82.9 ppm (C-3 of β-Gal*p*) in the HMBC spectrum (Fig. 7*B*). Both ROESY and HMBC confirmed that the Rib*f*A residues were attached to O-4 of Glc*p*A. Correlations were also found between Glc*p*A H1 and H4 (ROESY) and C4 (HMBC) of residues C and C′ (data not shown). The anomeric protons of residues E, E′, E″, and E_2' showed HMBC cross-peaks to C4 of residue F_3, which resonated near 75 ppm (Fig. 7). This chemical shift, which is unusually upfield for a 4-linked β-Glc residue, is due to the β-shielding effect of the *O*-acetyl group in the 3-position (43).

Because of overlap of the anomeric signals in the spectra, it was not possible to identify specific further connectivities between residues. However, the HMBC spectrum provided a way to define each residue more specifically (Fig. 7). Whereas the HSQC data identified the glycosylated position in each residue, the HMBC spectrum showed the linkage position of its reducing-side neighbor. In other words, each residue could be defined according to the form [→*x*-β-Glc-1→*y*], where *x* is the residue's own linkage (4 or 6), and *y* is the substituted position (3, 4, or 6) of its reducing-side neighbor. Each of the five Glc residues in the repeating unit is uniquely specified by this definition. Residue C is →4-β-Glc-1→6; residue D is →6-β-Glc-1→6; residue E is →6-β-Glc-1→4; residue F is →4-β-Glc-1→4;

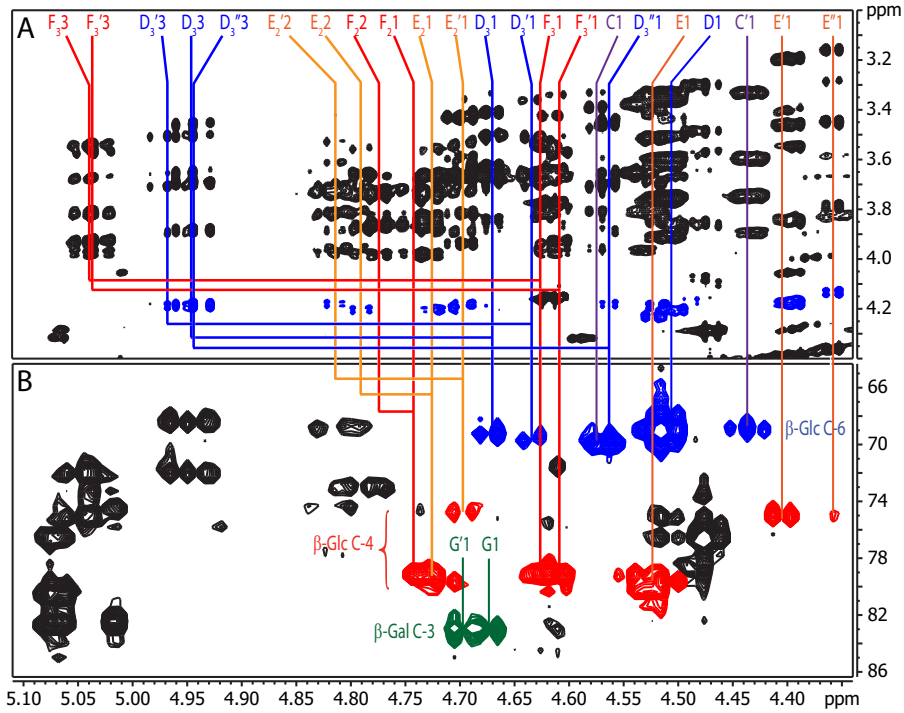

FIGURE 7. **Determination of the linkage positions *x* and *y* for each →*x*-*β*-Glc-1→*y* residue in the native octasaccharide.** The residues are labeled according to Table 3, and the numbers associated with the residue labels refer to the proton numbers, *e.g.* $E_2'2$ is H2 of residue E_2'. *A,* partial TOCSY spectrum with *β*-Glc anomeric proton signals and signals of protons in acetylated positions in F2 (direct dimension) and their coupling partners in F1 (indirect dimension). This spectrum identified 6-linked residues ($x = 6$) by the presence of downfield correlations around 4.2 ppm (in *blue*). The absence of such correlations indicated that the residue was 4-linked ($x = 4$). The downfield displacement of protons in acetylated positions allowed this identification because it removed their TOCSY sets from the crowded area of the spectrum. *B,* partial HMBC spectrum showing the same region in F2 as the TOCSY spectrum and the non-anomeric region in F1. Residues were distinguished by their correlations with peaks near 70 ppm ($y = 6$, *blue*), near 79 ppm ($y = 4$, *red*), or near 82 ppm ($y = 3$, *green*). Three correlations were near 74 ppm and corresponded to C4 of 3-*O*-acetylated 4-linked *β*-Glc. These were also color-coded in *red*. Spin systems are indicated by *colored lines* according to different *x,y*-combinations as follows: 4,4 (*red*), 4,6 (*purple*), 6,4 (*orange*), 6,6 (*blue*), and 4,3 (*green*). The *green lines* were shortened to avoid excessive crowding. For example, residue E_2 shows two sets of cross-peaks in the TOCSY spectrum, one correlating to H2 (designated $E_2$2), at 4.79 ppm in F2, and one correlating to H1 (designated $E_2$1), at 4.711 ppm in F2. Both of these sets include a cross-peak at 4.20 ppm, corresponding to H6 of residue E_2. The downfield chemical shift of this signal indicates that residue E_2 is 6-linked, *i.e.* $x = 6$. The HMBC spectrum shows a cross-peak correlating H1 of residue E_2 ($E_2$1) to a signal at 79.5 ppm, which is consistent with the chemical shift of C-4 of a *β*-glucose residue, therefore $y = 4$, and thus we conclude that residue E_2 is of the type 6→*β*-Glc-1→4.

and residue G is →4-*β*-Glc-1→3. This information made it possible to place all residues found in the native oligosaccharide in their proper positions in the previously determined *β*-Rib*f*A-(1→4)-*α*-Glc*p*A-(1→4)-*β*-Glc*p*-(1→6)-*β*-Glc*p*-(1→6)-*β*-Glc*p*-(1→4)-*β*-Glc*p*-(1→4)-*β*-Glc*p*-(1→3)-Gal*p* oligosaccharide sequence (Table 3). Table 4 summarizes annotations for all identified glycosyl residues in the *O*-acetylated octasaccharide. The anomeric protons of residues E, E′, E″, E‴, E_2, F_2, F_3, and F_3' displayed HMBC cross-peaks between 78 and 79 ppm, demonstrating their linkage to the 4-position of their neighbor, whereas residues C, C′, D, D_3, D_3', and D_3'' had HMBC correlations near 69 ppm, from their linkage to the 6-position of their neighbor. Residues G and G′ had H1/C3 cross-peaks to a carbon at 83 ppm, which is the Gal C3.

The results of NMR assignments and *O*-acetylation pattern in the octasaccharide were further supported by positive-mode Fourier transform ion cyclotron (FT-ICR) electrospray ionization (ESI) mass spectrometric analysis (supplemental Fig. 5 and supplemental Table 2). A distribution of up to four acetyl groups was observed in the LMM EPS octasaccharide $[RibAGlcAHex_6OAc_{(1-4)} + Na]^+$, with the majority of species possessing three *O*-acetyl substitutions consistent with results from negative-mode MALDI-MS analysis (Fig. 6). Interestingly, loss of the penturonic acid (residue A) from the major structure was accompanied with loss of one *O*-acetyl group, suggesting a conserved *O*-acetylation of the terminal RibA (supplemental Table 1, ions I and II). This was particularly observed in collision-induced dissociation MS/MS fragmentation of ion *m*/*z* 1461.4017, $[RibAGlcAHex_6OAc_3 + Na]^+$, by detection of a daughter ion at *m*/*z* 1273.3705 (IX) $[GlcAHex_6OAc_2 + Na]^+$, due to loss of RibA(OAc) (residue A) (supplemental Table 2 and supplemental Fig. 5).

Further assignments of R7A LMM EPS were possible by examination of the FT-ICR-ESI fragmentation pattern of a biotinylated derivative of the EPS octasaccharide (Fig. 8 and Table 5), which was recently used in plant receptor-EPS studies (40). We observed molecular ions ($[M + H]^+$ or $[M + 2H]^{2+}$) due to EPS octasaccharide conjugate $[RibAGlcAHex_6OAc_{(1-3)}$ LinkerBiotin$]^+$ carrying one to three *O*-acetyl groups. In addition, cleavage of residue A $[RibAOAc + H]^+$ from the main structure (fragment ion XIII) generated fragment ion I $[GlcAHex_6OAc_2LinkerBiotin + H]^+$ and fragment ion II $[GlcAHex_6OAcLinkerBiotin + H]^+$ due to heptasaccharides (residues B-H) with two or one *O*-acetyl substitutions, respectively. Assuming RibA is *O*-acetylated, residues B and C were deduced to be non-acetylated by detection of [RibAGlcA-

TABLE 3

Proton ^{1}H and carbon ^{13}C chemical shift assignments of the native R7A*ndvB* LMM oligosaccharide

The subscript number indicates position of *O*-acetyl group in glycosyl residue, *i.e.* A_3 indicates mono-3-*O*-acetylated β-Rib*f*A; $A_{2,3}$ indicates 2,3-di-O-Ac-β-Rib*f*A; E, E′, and E″, or D_3, D_3', and D_3'' indicates different variants of same monosaccharide residue observed in NMR experiments due to different substitution patterns by *O*-acetyl groups on neighboring residues. All presented monosaccharides have -D- configuration; ND not detected.

	Residue	H1 C1	H2 C2	H3 C3	H4 C4	H5 C5	H6a C6	H6b
A	β-Rib*f*A	5.01	4.05	4.39	4.29			
		109.3	75.3	74.8	84.4	178.4		
A_3	3-O-Ac-β-Rib*f*A	5.06	4.28	5.28	4.47			
		109.8	73.8	76.3	80.4	177.4		
$A_{2,3}$	2,3-di-O-Ac-β-Rib*f*A	5.16	5.07	4.59	4.32			
		106.8	77.3	73.3	83.4	177.9		
B	4-α-Glc*p*A-(1→4)	5.33	3.67	3.75	3.55	4.02		
		100.2	71.2	71.8	82.4	72.8	174.8	
C	4-β-Glc*p*-(1→6)	4.574	3.39	3.32	3.70	3.47	3.95	3.81
		103.2	73.7	73.7	79.9	76.1	60.5	
C′	4-β-Glc*p*-(1→6)	4.431	3.33	3.74	3.58	ND	ND	ND
		103.1	73.4	76.3	78.5	ND	ND	
D	6-β-Glc*p*-(1→6)	4.502	3.36	3.61	3.50	3.75	4.20	3.91
		103.2	72.8	75.3	71.2	76.3	68.7	
D_3	3-O-Ac-6-β-Glcp-(1→6)	4.673	3.51	4.94	3.65	3.69	4.18	3.88
		103.7	74.8	77.3	71.2	75.3	68.7	
$D_{3'}$	3-O-Ac-6-β-Glc*p*-(1→6)	4.638	3.50	4.96	3.65	3.71	4.19	3.89
		102.7	74.8	77.3	71.2	75.3	68.7	
$D_{3''}$	3-O-Ac-6-β-Glc*p*-(1→6)	4.561	3.45	4.94	3.65	3.7	4.18	3.88
		103.2	73.2	77.8	71.2	75.3	68.7	
E	6-β-Glc*p*-(1→4)	4.519	3.33	3.60	3.51	3.75	4.23	3.90
		103.2	73.0	75.3	71.8	76.3	68.7	
E′	6-β-Glc*p*-(1→4)	4.397	3.20	3.46	3.40	3.55	4.18	3.85
		102.2	73.8	75.9	70.2	76.1	69.5	
E″	6-β-Glc*p*-(1→4)	4.356	3.15	3.46	3.28	3.46	4.13	3.80
		102.3	73.9	75.9	70.2	76.1	69.7	
E‴	6-β-Glc*p*-(1→4)	4.500	3.32	3.60	3.51	3.75	4.21	3.91
		103.2	73.0	75.3	71.8	76.3	68.7	
E_2	2-O-Ac-6-β-Glc*p*-(1→4)	4.711	4.79	3.86	ND	ND	4.20	ND
		103.7	74.2	72.8	ND	ND	68.7	
$E_{2'}$	2-O-Ac-6-β-Glc*p*-(1→4)	4.695	4.81	3.81	ND	ND	4.18	3.88
		103.7	71.2	73.3	ND	ND	68.7	
F_2	2-O-Ac-4-β-Glc*p*-(1→4)	4.721	4.77	3.86	3.67	3.74	3.97	3.82
		100.7	73.8	72.8	78.7	76.3	60.6	
F_3	3-O-Ac-4-β-Glc*p*-(1→4)	4.622	3.54	5.04	3.93	ND	ND	ND
		102.7	71.7	75.8	74.8	ND	ND	
$F_{3'}$	3-O-Ac-4-β-Glc*p*-(1→4)	4.606	3.57	5.04	3.83	ND	ND	ND
		102.7	71.7	75.3	73.3	ND	ND	
G	4-β-Glc*p*-(1→3)	4.689	3.41	3.67	3.63	3.5	3.83	3.67
		103.7	73.8	74.8	78.9	75.8	60.6	
G′	4-β-Glc*p*-(1→3)	4.697	3.43	3.67	3.67	ND	ND	ND
		103.7	73.8	74.8	78.8	ND	ND	
Hβ	3-β-Gal*p*	4.613	3.65	3.79	4.15	3.69	ND	ND
		96.6	71.2	82.9	68.7	75.3	ND	
Hα	3-α-Gal*p*	5.27	3.97	3.97	4.22	4.09	3.72	3.72
		92.1	67.7	79.9	69.2	70.7	61.1	

TABLE 4

Placement of individual (acetylated and unsubstituted) monosaccharide residues in the oligosaccharide sequence of LMM R7A EPS (also refer to structure in Fig. 9)

Numbers in parentheses indicate a position of *O*-acetyl substituent on glycosyl residue; (0) indicates non-*O*-acetylated residue; subscript number indicates position of *O*-acetyl group in glycosyl residue, i.e. A_3 indicates mono-3-*O*-acetylated β-Rib*f*A; $A_{2,3}$ indicates 2,3-di-*O*-acetylated β-Rib*f*A; ′, i.e. E, E′, E″, E‴, E2, E2′, or D3, D3′, D3″, indicates different variants of same monosaccharide residue observed in NMR experiments due to different substitution patterns by *O*-acetyl groups on neighboring residues.

Residue							
A	**B**	**C**	**D**	**E**	**F**	**G**	**H**
β-Rib*f*A-1→4-β-Glc*p*A-1→4-β-Glc*p*-1→6-β-Glc*p*-1→6-β-Glc*p*-1→4-β-Glc*p*-1→4-β-Glc*p*-1→3-β-Gal*p*							
(0) A	(0) B	(0) C	(0) D	(0) E	(2) F_2	(0) G	(0) H
(3) A_3		(0) C′	(3) D_3	(0) E′	(3) F_3	(0) G′	
(2,3) $A_{2,3}$			(3) D_3'	(0) E″	(3) F_3'		
			(3) D_3''	(0) E‴			
				(2) E_2			
				(2) E_2'			

HexOAc + H]$^+$ (fragment ion XII). The identification of [GlcAHex_6OAc_2LinkerBiotin + 2H]$^{2+}$ (fragment ion I) and [Hex_5OAc_2LinkerBiotin + H]$^+$ (fragment ion III), and fragments [Hex_3OAcLinkerBiotin + H]$^+$ (fragment ion VII) and [Hex_4OAcLinkerBiotin + H]$^+$ (fragment ion V), indicated the presence of an *O*-acetyl group on residue D as well as

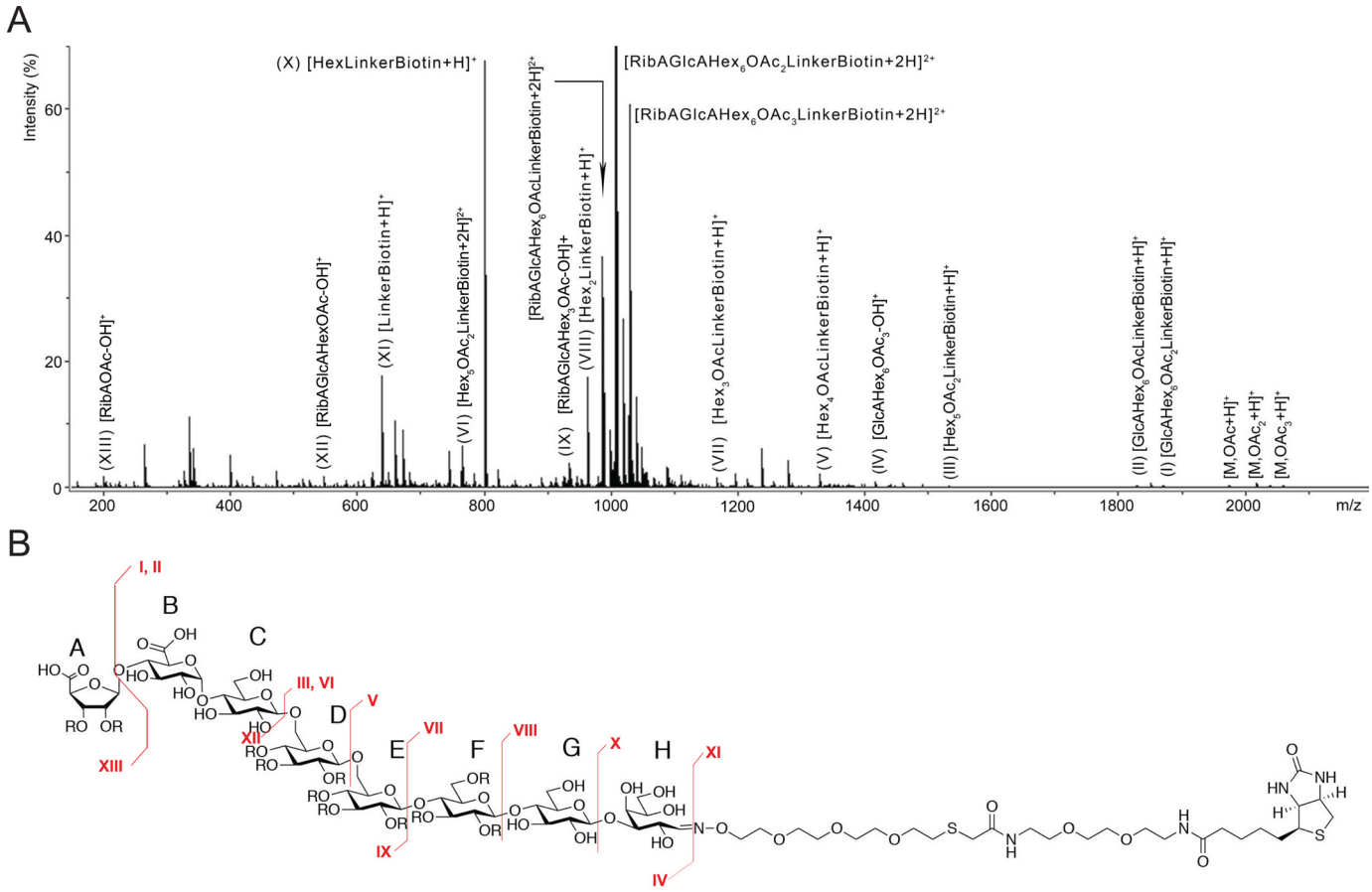

FIGURE 8. **XR ESI/MALDI-FT-ICR-MS analysis of EPS octasaccharide conjugate, with fragmentation ions indicated with roman numerals *I–XIII* as listed in Table 5 (*A*) and proposed ICR-MS fragments (*B*).** "*R*" in the structure in *B* indicates possible location of acetyl groups in place of hydrogen.

on either of residues E or F. Furthermore, identification of $[HexLinkerBiotin + H]^+$ (fragment ion X) and $[Hex_2LinkerBiotin + H]^+$ showed that residues G and H were non-acetylated (Fig. 8, *A* and *B*). Fragment ions are summarized in Table 5.

Considering all NMR, MALDI-MS, FT-ICR ESI MS and MS/MS, and glycosyl linkage results together, we conclude that the LMM EPS consists of eight glycosyl residues in the sequence shown in Table 4 and Fig. 9. The *O*-acetylation of the octasaccharide occurs only at four glycosyl residues (A and D–F), and only at specific *O*-positions within those residues. Thus, Rib*f*A at the non-reducing end (residue A) is partially acetylated on O-3 or di-acetylated on O-2 and O-3; the 6-β-Glc*p* (residue D) is partially acetylated at O-3, the 6-β-Glc*p* (residue E) is partially acetylated on O-2, and the 4-β-Glc*p* (residue F) is either 2- or 3-*O*-acetylated. Despite the structural microheterogeneity, the majority of the LMM EPS is represented by an octasaccharide unit substituted with three *O*-acetyl groups. The octasaccharide has the same sequence as the HMM polymer and thus we propose that it represents a single biosynthetic subunit of HMM EPS.

Discussion

M. loti strain R7A is a microsymbiont of the model legume *L. japonicus*. Recent studies using this model system have indicated wild-type rhizobial EPS plays a role in enhancing the establishment of the determinate symbiosis, whereas truncated EPS produced by certain R7A *exo* mutants (*e.g. exoU*) plays a negative role and prevents the establishment of infection threads and their passage through the epidermal cell layer. It is proposed that LMM forms of both types of EPS are perceived by the LysM receptor-like kinase, EPR3, to regulate infection thread passage. Genetic evidence using rhizobial mutants (38) indicates that the positive function of wild-type EPS is dominant over the negative effect of truncated EPS, but whether this reflects different binding affinities of the two types of EPS to EPR3 remains to be determined. The detailed structures of both HMM and LMM EPS reported in this study are crucial for the biochemical characterization and understanding of the molecular mechanisms by which EPS is perceived in symbiosis. Structural studies of EPS are also important for characterization of the various phenotypes observed with *M. loti exo* mutants and for understanding the differences between symbiotically compatible and incompatible EPS, which may explain some of the variation in symbiotic efficiencies seen between rhizobial strains producing very similar Nod factors.

In this work, we show that the repeating oligosaccharide unit of HMM EPS and LMM EPS oligosaccharide share a similar structure in that they consist of highly *O*-acetylated (2,3/3-OAc)β-D-Rib*f*A-(1→4)-α-D-Glc*p*A-(1→4)-β-D-Glc*p*-(1→6)-(3-OAc)β-D-Glc*p*-(1→6)-*[(2-OAc)β-D-Glc*p*-(1→4)-(2/3-OAc)β-D-Glc*p*-(1→4)-β-D-Glc*p*-(1→3)-β-D-Gal*p*]. Every new repeating unit is attached via its reducing-end β-D-Gal*p* to C-4

TABLE 5

High resolution MS analysis of biotin conjugate of *M. loti* R7A EPS octasaccharide and proposed compositions

For mass spectra and structure assignments refer to Fig. 8.

HR-MS of EPS-Linker-Biotin Conjugate							
		Residues	Composition	OAc groups	Calcd.	Found	Δ (ppm)
		A-H-linker-biotin	$[RibAGlcAHex_6OAc_3LinkerBiotin+H]^+$	3	2060.7067	2060.7066	0.04
		A-H-linker-biotin	$[RibAGlcAHex_6OAc_2LinkerBiotin+H]^+$	2	2018.6961	2018.7004	-2.13
		A-H-linker-biotin	$[RibAGlcAHex_6OAcLinkerBiotin+H]^+$	1	1976.6856	1976.6888	-1.61
		A-H-linker-biotin	$[RibAGlcAHex_6OAc_3LinkerBiotin+2H]^{2+}$	3	1030.8574	1030.8559	1.45
		A-H-linker-biotin	$[RibAGlcAHex_6OAc_2LinkerBiotin+2H]^{2+}$	2	1009.8521	1009.8514	0.69
		A-H-linker-biotin	$[RibAGlcAHex_6OAcLinkerBiotin+2H]^{2+}$	1	988.8468	988.8463	0.50
Fragmentation ion							
No.	Type						
I	Y_7	B-H-linker-biotin	$[GlcAHex_6OAc_2LinkerBiotin+H]^+$	2	1872.6746	1872.6786	-2.15
II	Y_7	B-H-linker-biotin	$[GlcAHex_6OAcLinkerBiotin+H]^+$	1	1830.6640	1830.6674	-1.89
III	Y_5	D-H-linker-biotin	$[Hex_5OAc_2LinkerBiotin+H]^+$	2	1534.5897	1534.5905	-0.52
IV	B_8	A-H	$[GlcAHex_6OAc_3\text{-}OH]^+$	3	1421.4095	1421.4089	0.42
V	Y_4	E-H-linker-biotin	$[Hex_4OAcLinkerBiotin+H]^+$	1	1330.5263	1330.5281	-1.35
VI	Y_5	D-H-linker-biotin	$[Hex_5OAc_2LinkerBiotin+2H]^{2+}$	2	767.7985	767.7985	-0.01
VII	Y_3	F-H-linker-biotin	$[Hex_3OAcLinkerBiotin+H]^+$	1	1168.4735	1168.4739	-0.34
VIII	Y_2	G-H-linker-biotin	$[Hex_2LinkerBiotin+H]^+$	0	964.4101	964.4101	-0.04
IX	B_5	A-E	$[RibAGlcAHex_3OAc_2\text{-}OH]^+$	2	893.2405	893.2360	5.03
X	Y_1	H-linker-biotin	$[HexLinkerBiotin+H]^+$	0	802.3573	802.3569	0.49
XI	Y_0	Biotin-Linker	$[LinkerBiotin+H]^+$	n/a	640.3045	640.3044	0.15
XII	B_3	A-C	$[RibAGlcAHexOAc\text{-}OH]^+$	1	527.1243	527.1242	0.18
XIII	B_1	A	$[RibAOAc\text{-}OH]^+$	1	189.0394	189.0394	0.00

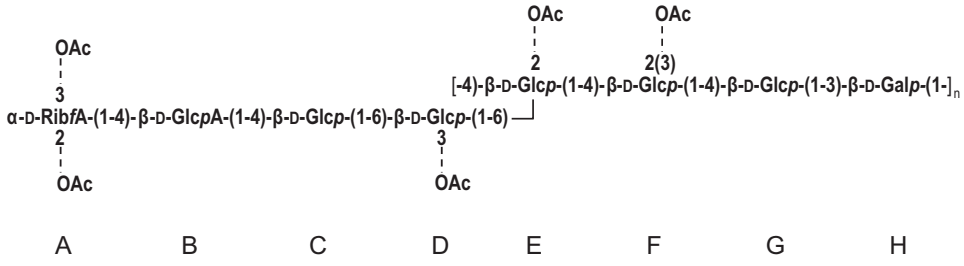

FIGURE 9. **Proposed structure of *O*-acetylated octasaccharide subunit of polymeric EPS from *M. loti* R7A.** An average EPS octasaccharide is non-stoichiometrically substituted by three *O*-acetyl groups at different glycosyl residues (indicated by *dashed line*).

of fourth glucose (asterisked above) of that octasaccharide in the formation of the polysaccharide. The terminal residue of the branching oligosaccharide was found to be D-riburonic acid, which to our knowledge has only been reported in EPS from one other microorganism, reported as *Rhizobium* (*Sinorhizobium*) *meliloti* IFO 13336 (44). Indeed, the structure of the carbohydrate portion of R7A EPS is consistent with that reported for IFO 13336, with the exception that the branched-chain terminal Rib*f*A in R7A was β-D-Rib*f*A and not α-D-Rib*f*A, and the presence and location of the *O*-acetyl groups were not determined in IFO 13336 EPS. Amemura *et al.* (44) determined their structure using a method involving successive fragmentation with two β-D-glycanases, and hence their study provides strong complementary support for the structure reported in this paper. Also, Amemura *et al.* (44) concluded that Rib*f*A is in the α-anomeric configuration because the NMR chemical shift of its anomeric proton is greater than 5 ppm. However, the anomeric proton chemical shifts of aldofuranoses tend to be greater than 5 ppm in both α- and β-anomeric configurations (45, 46). Given the similarities of R7A and IFO 13336 EPS, it seems likely that IFO 13336 was misidentified as *S. meliloti,* and indeed the strain is listed as belonging to *Mesorhizobium* sp. in the NITE Biological Resource Center (NBRC) Culture Collection.

We identified heterogeneity in EPS *O*-acetylation, showing that on average an octasaccharide unit is substituted with three *O*-acetyl groups out of six possible *O*-acetylation sites within four glycosyl residues (Table 4 and Fig. 9). *O*-Acetyl groups are well known to migrate between neighboring hydroxyl groups of carbohydrates (47). Therefore, it is possible that the variability in location is due to chemical rearrangement rather than specific enzymatic action. Although migration from O-3 to O-4 is

precluded in the 4-linked residues, it would be possible in 6-linked residues and in fact has been observed in Glc monomers (48). However, the complete absence of 4-*O*-acetylation in any of the residues observed in the octasaccharide indicates that migration is likely not a factor. The genetic basis for the addition of the three *O*-acetyl groups remains to be identified. The structures of *M. loti* EPS, succinoglycan from *S. meliloti* 1021, and EPS from *Rhizobium tropici* CIAT 899 (16–20, 49) share many similarities. In this type of EPS polymer, every new octasaccharide subunit attaches via its reducing-end Gal to C4 of the fourth glycosyl residue of the polymer. In most of the octasaccharide polymers identified thus far, it is a branching 4,6-glucose. Hence, each EPS subunit consists of an *O*-acetylated tetrasaccharide repeating backbone with the remaining glycosyl residues forming the branching tetrasaccharide. The backbone tetrasaccharide and the two first side-chain residues seem to be conserved in these rhizobial strains. The proteins required for the assembly of this hexasaccharide (ExoY, -A, -L, -M, -O, and -U) have been identified for succinoglycan (13, 50). The genetic organization of the corresponding genes is also conserved among the three species, which all make EPS with an octasaccharide repeating unit, and also *S. fredii* strains NGR234 and HH103, which make an EPS with a nonasaccharide repeating unit (compare structures in Figs. 1 and 9 with supplemental Fig. 6) (25, 51) and a six-residue backbone. Interestingly, this backbone is identical to the hexasaccharide described above, and the three-residue branch is attached to the fifth residue of the backbone. Hence, several diverse rhizobia synthesize similar EPS with the differences restricted to the last two or three residues of the branch and the types and positioning of the non-carbohydrate substituents. It seems likely that these differences play a critical role in host specificity during establishment of the rhizobium-legume symbiosis. Currently, nothing is known about the biological properties bestowed on the EPS by riburonic acid or the mechanisms by which it is synthesized and added to the EPS. In addition, the gene(s) required for the addition of glucuronic acid to the *M. loti* EPS are unknown. We are currently addressing these questions.

The branch chains of the EPS discussed above contribute to the acidic character of the EPS (uronic acids, pyruvylated or succinylated neutral sugars) as well as their sequence heterogeneity. Although the functions of non-carbohydrate modifications of rhizobial EPS are not fully understood, there is evidence of a pivotal role in the symbiosis. In an *S. meliloti exoZ* mutant defective in expression of acetyltransferase, lack of *O*-acetylation of succinoglycan caused increased susceptibility of the polymer to cleavage by endogenous ExoK and ExsH endo-1,3–1,4-β-glycanases. This resulted in increased production of LMM EPS, thus suggesting that *O*-acetylation may play a regulatory role in EPS length modifications. In contrast, an *exoH* mutant defective in succinylation produced only HMM EPS (37, 52, 53). The *exoZ* mutant was able to establish symbiosis with alfalfa but with reduced efficiency of infection thread formation and reduced nodule invasion (36, 54), whereas the *exoH* mutant was unable to initiate infection thread formation. Lack of pyruvylation of succinoglycan caused by an *exoV* mutation resulted in the production of only monomer units, indicating pyruvylation is required for succinoglycan polymerization (50). In other bacteria, acetyl groups may also contribute to rheological, conformational, and physical properties of EPS. These changes provide protection, allowing early stages of biofilm formation, cell aggregation, and steric prevention of enzymatic degradation by soil microorganisms (55, 56). Therefore, they may perform similar functions in rhizobia.

The LMM EPS characterized in this work is a monomeric octasaccharide with an average of three acetyl group substitutions. This octasaccharide is recognized by the plant EPR3 kinase receptor resulting in a positive response (40). It seems likely that the polysaccharide produced by the *M. loti exoU* mutant that initiates a negative response from the EPR3 receptor is a pentasaccharide with reduced acetylation and acidity compared with the octasaccharide. It will be of interest to determine the role of the *O*-acetyl groups as well as the effect of polysaccharide chain length on molecular recognition by the receptor and to determine how these opposing responses control passage through the root hair and the infection process.

A signaling role of LMM EPS in the symbiotic interaction with plants was also proposed for *S. meliloti* 1021 and *S. fredii* NGR234. In the case of *S. meliloti*, a trimer repeat of the octasaccharide was the most symbiotically active molecule (20, 34), whereas only monomeric octa- and nonasaccharides were identified for NGR234, indicating these were the symbiotically active species (26). However, recent studies on succinoglycan in *S. meliloti* 1021 suggest no requirement for LMM EPS in host invasion in indeterminate symbiosis and a more critical role of succinylation of the polysaccharide rather than molecular size (35). Our discovery that only an acetylated octasaccharide monomer is found in the crude LMM fraction rather than dimers or trimers of the repeating octasaccharide is in agreement with the data reported for *S. fredii* NGR234 (26), suggesting that a LMM EPS size requirement for symbiotic interaction could be both microbe- and host plant-dependent. Further studies on symbiotically compatible and incompatible exopolysaccharides and their contrasting effects on EPR3-mediated control of the rhizobial infection processes are underway.

Experimental Procedures

Isolation and Purification of M. loti R7A EPS—The wild type and an *ndv*B mutant of *M. loti* strain R7A, strain R7AndvB (38), which does not make cyclic β-glucans, were used for the isolation of EPS. The strains were grown in glucose/rhizobium-defined medium (*Rhizobium* defined medium containing 10 mM glucose) (38), and HMM EPS was precipitated from stationary phase culture supernatants with 3 volumes of ethanol (EtOH) and purified by chromatography as described previously (38). Traces of cyclic β-glucan were removed from chromatographed HMM EPS by extensive dialysis against H_2O using a 50,000-Da MWCO dialysis tubing. The supernatant recovered from the 3-volume EtOH HMM EPS precipitation was concentrated by rotary evaporation, and 9 volumes of EtOH (v/v) were added, allowed to stand overnight at 4 °C, and centrifuged at 5000 × *g* for 20 min to form crude LMM EPS precipitate. The crude LMM was desalted and purified from monomeric glucose on a Bio-Gel P2 column (120 × 1.5-cm inner diameter) or by dialysis against H_2O using 1000-Da MWCO dialysis tubing and was later resolved on a Superdex Peptide 10/300 FPLC

column with 50 mM ammonium acetate used as eluent. Eluting fractions were monitored by refractive index and by a multiple wavelength detector (Agilent Technologies 1200) at 210, 230, and 280 nm.

Chemical Composition Analysis—To identify the glycosyl residues in the EPS, trimethylsilyl methyl glycosides were prepared as described previously (38, 57). The linkage analysis of neutral sugars and uronic acids was done by preparing and analyzing PMAAs (57) or PMAAs prepared after mild methyl carboxyl esterification and reduction of uronic acids prior to permethylation. The details of this chemical modification were previously reported (38). Stereochemical configuration of the glycosyl residues was performed following the method of Gerwig *et al.* (39, 58) with optically active (*S*)-(+)-2-butanol (Sigma).

De-O-acetylation of EPS—HMM and LMM EPS were de-*O*-acetylated in 12.5% NH_4OH for 12 h at 35 °C. Alternatively samples were de-*O*-acetylated with 10 mM KOH for 5 h at 20 °C, and the reaction was quenched with HCl. Salts were removed by dialysis (1000-Da MWCO) against several changes of deionized water.

Mass Spectrometric Analysis of Native LMM EPS—The LMM EPS fraction was recovered from the 9-volume EtOH precipitate and Superdex Peptide 10/300 column, respectively, dissolved in water, mixed 1:1 (v/v) with 0.5 M 2,4,6-trihydroxyacetophenone monohydrate matrix in methanol, and spotted onto a MALDI plate. MALDI-TOF MS spectra were acquired on an Applied Biosystems AB SCIEX TOF/TOF 5800 system in the negative reflectron detection-mode and processed with Data Explorer (Applied Biosystems). High resolution mass spectrometry was performed on a Bruker Solarix XR ESI/MALDI-FT-ICR-MS instrument equipped with a 7-tesla magnet. Spectra were acquired in the positive ESI-mode, externally calibrated with NaOTFA cluster ions, and processed using Bruker Data Analysis version 4.1.

NMR Analysis of EPS—Native and de-*O*-acetylated HMM and LMM EPS were exchanged twice in 99.9% D_2O and finally dissolved in 100% D_2O (Cambridge Isotope Laboratories, Andover, MA) at a final concentration of 6 mg/ml. 1D proton and 2D ^1H-^1H (COSY, TOCSY, NOESY, ROESY, and ^1H-^{13}C (HSQC and HMBC) spectra were acquired at 70 °C on a Varian 600 MHz spectrometer equipped with 3-mm cold probe and processed using MestReC/Nova software (Mestrelab Research, Santiago de Compostela, Spain). For 2D acquisitions, the solvent signal was suppressed with a standard solvent suppression experiment in one-dimensional proton NMR. COSY experiments were recorded using sets of 1024 time increments with 8 scans per increment and an acquisition time of 0.4 s. TOCSY experiments were recorded using sets of 256 time increments with 32 scans per increment, acquisition time of 0.4 s, and 1-s saturation delay. NOESY experiments were recorded with a mixing time of 0.12 s, sets of 128 increments with 64 scans per increment, and an acquisition time of 0.4 s. The ROESY experiment was recorded with a mixing time of 0.2 s, sets of 512 increments with 16 scans per increment, and an acquisition time of 0.4 s. Proton-carbon multiplicity edited HSQC experiments were recorded using sets of 128 time increments with 128 scans per increment and an acquisition time of 0.2 s. HMBC experiments were recorded using sets of 256 time increments with 128 scans per increment and an acquisition time of 0.2 s. All experiments were performed using a saturation delay of 1 s. Spectra were calibrated to internal standards of acetone and tetramethylsilane.

Author Contributions—A. M., R. W. C., J. S., and C. W. R. conceived and coordinated the study. A. M., C. T. H., S. J.K., and J. T. S. performed the experiments. A. M., C. H., C. T. H., R. W. C., and M. B. T. analyzed the results and interpreted the data. A. M., C. H., C. W. R., R. W. C., C. T. H., M. B. T., J. S., and P. A. wrote the manuscript. All authors reviewed the results and approved the final version of the manuscript.

Acknowledgment—We thank Dr. Theis Brock-Nannestad for help with XR FT-ICR mass spectrometry.

References

1. Perret, X., Staehelin, C., and Broughton, W. J. (2000) Molecular basis of symbiotic promiscuity. *Microbiol. Mol. Biol. Rev.* **64,** 180–201
2. Rodpothong, P., Sullivan, J. T., Songsrirote, K., Sumpton, D., Cheung, K. W. J. T., Thomas-Oates, J., Radutoiu, S., Stougaard, J., and Ronson, C. W. (2009) Nodulation gene mutants of *Mesorhizobium loti* R7A–nodZ and nolL mutants have host-specific phenotypes on *Lotus spp. Mol. Plant. Microbe Interact.* **22,** 1546–1554
3. Radutoiu, S., Madsen, L. H., Madsen, E. B., Felle, H. H., Umehara, Y., Grønlund, M., Sato, S., Nakamura, Y., Tabata, S., Sandal, N., and Stougaard, J. (2003) Plant recognition of symbiotic bacteria requires two LysM receptor-like kinases. *Nature* **425,** 585–592
4. Madsen, E. B., Madsen, L. H., Radutoiu, S., Olbryt, M., Rakwalska, M., Szczyglowski, K., Sato, S., Kaneko, T., Tabata, S., Sandal, N., and Stougaard, J. (2003) A receptor kinase gene of the LysM type is involved in legume perception of rhizobial signals. *Nature* **425,** 637–640
5. Limpens, E., Franken, C., Smit, P., Willemse, J., Bisseling, T., and Geurts, R. (2003) LysM domain receptor kinases regulating rhizobial Nod factor-induced infection. *Science* **302,** 630–633
6. Madsen, L. H., Tirichine, L., Jurkiewicz, A., Sullivan, J. T., Heckmann, A. B., Bek, A. S., Ronson, C. W., James, E. K., and Stougaard, J. (2010) The molecular network governing nodule organogenesis and infection in the model legume *Lotus japonicus. Nat. Commun.* **1,** 10
7. Xie, F., Murray, J. D., Kim, J., Heckmann, A. B., Edwards, A., Oldroyd, G. E., and Downie, J. A. (2012) Legume pectate lyase required for root infection by rhizobia. *Proc. Natl. Acad. Sci. U.S.A.* **109,** 633–638
8. Fournier, J., Teillet, A., Chabaud, M., Ivanov, S., Genre, A., Limpens, E., de Carvalho-Niebel, F., and Barker, D. (2015) Remodeling of the infection chamber prior to infection thread formation reveals a two-step mechanism for rhizobial entry into the host legume root hair. *Plant Physiol.* **167,** 1233–1242
9. Desbrosses, G. J., and Stougaard, J. (2011) Root nodulation: a paradigm for how plant-microbe symbiosis influences host developmental pathways. *Cell Host Microbe* **10,** 348–358
10. Gibson, K. E., Kobayashi, H., and Walker, G. C. (2008) Molecular determinants of a symbiotic chronic infection. *Annu. Rev. Genet.* **42,** 413–441
11. Carlson, R. W., Forsberg, L. S., and Kannenberg, E. L. (2010) *Endotoxins: Structure, Function and Recognition*, pp. 339–386, Springer, Netherlands
12. Broughton, W. J., Jabbouri, S., and Perret, X. (2000) Keys to symbiotic harmony. *J. Bacteriol.* **182,** 5641–5652
13. Skorupska, A., Janczarek, M., Marczak, M., Mazur, A., and Król, J. (2006) Rhizobial exopolysaccharides: genetic control and symbiotic functions. *Microb. Cell Fact.* **5,** 7
14. Fraysse, N., Couderc, F., and Poinsot, V. (2003) Surface polysaccharide involvement in establishing the rhizobium–legume symbiosis. *Eur. J. Biochem.* **270,** 1365–1380
15. Janczarek, M., Rachwał, K., Marzec, A., Grządziel, J., and Palusińska-Szysz, M. (2015) Signal molecules and cell-surface components involved

in early stages of the legume-rhizobium interactions. *Appl. Soil Ecol.* **85,** 94–113
16. Åman, P., McNeil, M., Franzén, L. E., and Darvill, A. G., and Albersheim, P. (1981) Structural elucidation, using HPLC-MS and GLC-MS, of the acidic polysaccharide secreted by *Rhizobium meliloti* strain 1021. *Carbohydr. Res.* **95,** 263–282
17. Reinhold, B. B., Chan, S. Y., Reuber, T. L., Marra, A., Walker, G. C., and Reinhold, V. N. (1994) Detailed structural characterization of succinoglycan, the major exopolysaccharide of *Rhizobium meliloti* Rm1021. *J. Bacteriol.* **176,** 1997–2002
18. Chouly, C., Colquhoun, I. J., Jodelet, A., York, G., and Walker, G. C. (1995) NMR studies of succinoglycan repeating-unit octasaccharides from *Rhizobium meliloti* and *Agrobacterium radiobacter*. *Int. J. Biol. Macromol.* **17,** 357–363
19. Zevenhuizen, L. P., and van Neerven, A. R. (1983) (1→2)-β-D-glucan and acidic oligosaccharides produced by *Rhizobium meliloti*. *Carbohydr. Res.* **118,** 127–134
20. Wang, L. X., Wang, Y., Pellock, B., and Walker, G. C. (1999) Structural characterization of the symbiotically important low-molecular-weight succinoglycan of *Sinorhizobium meliloti*. *J. Bacteriol.* **181,** 6788–6796
21. Her, G.-R., Glazebrook, J., Walker, G. C., and Reinhold, V. N. (1990) Structural studies of a novel exopolysaccharide produced by a mutant of *Rhizobium meliloti* strain Rm1021. *Carbohydr. Res.* **198,** 305–312
22. Philip-Hollingsworth, S., Hollingsworth, R. I., Dazzo, F. B., Djordjevic, M. A., and Rolfe, B. G. (1989) The effect of interspecies transfer of *Rhizobium* host-specific nodulation genes on acidic polysaccharide structure and in situ binding by host lectin. *J. Biol. Chem.* **264,** 5710–5714
23. Robertsen, B. K., Aman, P., Darvill, A. G., McNeil, M., and Albersheim, P. (1981) Host-Symbiont interactions: V. The structure of acidic extracellular polysaccharides secreted by *Rhizobium leguminosarum* and *Rhizobium trifolii*. *Plant Physiol.* **67,** 389–400
24. O'Neill, M. A., Darvill, A. G., and Albersheim, P. (1991) The degree of esterification and points of substitution by *O*-acetyl and *O*-(3-hydroxybutanoyl) groups in the acidic extracellular polysaccharides secreted by *Rhizobium leguminosarum* biovars *viciae*, trifolii, and *phaseoli* are not related to host range. *J. Biol. Chem.* **266,** 9549–9555
25. Djordjevic, S. P., Rolfe, B. G., Batley, M., and Redmond, J. W. (1986) The structure of the exopolysaccharide from *Rhizobium* sp. strain ANU280 (NGR234). *Carbohydr. Res.* **148,** 87–99
26. Staehelin, C., Forsberg, L. S., D'Haeze, W., Gao, M.-Y., Carlson, R. W., Xie, Z.-P., Pellock, B. J., Jones, K. M., Walker, G. C., Streit, W. R., and Broughton, W. J. (2006) Exo-oligosaccharides of *Rhizobium sp.* Strain NGR234 are required for symbiosis with various legumes. *J. Bacteriol.* **188,** 6168–6178
27. Battisti, L., Lara, J. C., and Leigh, J. A. (1992) Specific oligosaccharide form of the *Rhizobium meliloti* exopolysaccharide promotes nodule invasion in alfalfa. *Proc. Natl. Acad. Sci. U.S.A.* **89,** 5625–5629
28. Urzainqui, A., and Walker, G. C. (1992) Exogenous suppression of the symbiotic deficiencies of *Rhizobium meliloti* exo mutants. *J. Bacteriol.* **174,** 3403–3406
29. Lehman, A. P., and Long, S. R. (2013) Exopolysaccharides from *Sinorhizobium meliloti* can protect against H_2O_2-dependent damage. *J. Bacteriol.* **195,** 5362–5369
30. Laus, M. C., van Brussel, A. A., and Kijne, J. W. (2005) Role of cellulose fibrils and exopolysaccharides of *Rhizobium leguminosarum* in attachment to and infection of *Vicia sativa* root hairs. *Mol. Plant. Microbe Interact.* **18,** 533–538
31. Aslam, S. N., Newman, M. A., Erbs, G., Morrissey, K. L., Chinchilla, D., Boller, T., Jensen, T. T., De Castro, C., Ierano, T., Molinaro, A., Jackson, R. W., Knight, M. R., and Cooper, R. M. (2008) Bacterial polysaccharides suppress induced innate immunity by calcium chelation. *Curr. Biol.* **18,** 1078–1083
32. Djordjevic, S. P., Chen, H., Batley, M., Redmond, J. W., and Rolfe, B. G. (1987) Nitrogen fixation ability of exopolysaccharide synthesis mutants of *Rhizobium* sp. strain NGR234 and *Rhizobium trifolii* is restored by the addition of homologous exopolysaccharides. *J. Bacteriol.* **169,** 53–60
33. Gonzalez, J. E., Reuhs, B. L., and Walker, G. C. (1996) Low molecular weight EPS II of *Rhizobium meliloti* allows nodule invasion in *Medicago sativa*. *Proc. Natl. Acad. Sci. U.S.A.* **93,** 8636–8641
34. Gonzalez, J. E., Semino, C. E., Wang, L. X., Castellano-Torres, L. E., and Walker, G. C. (1998) Biosynthetic control of molecular weight in the polymerization of the octasaccharide subunits of succinoglycan, a symbiotically important exopolysaccharide of *Rhizobium meliloti*. *Proc. Natl. Acad. Sci. U.S.A.* **95,** 13477–13482
35. Mendis, H. C., Madzima, T. F., Queiroux, C., and Jones, K. M. (2016) Function of succinoglycan polysaccharide in *Sinorhizobium meliloti* host plant invasion depends on succinylation, not molecular weight. *mBio* 10.1128/mBio.00606–16
36. Cheng, H. P., and Walker, G. C. (1998) Succinoglycan is required for initiation and elongation of infection threads during nodulation of alfalfa by *Rhizobium meliloti*. *J. Bacteriol.* **180,** 5183–5191
37. York, G. M., and Walker, G. C. (1998) The succinyl and acetyl modifications of succinoglycan influence susceptibility of succinoglycan to cleavage by the *Rhizobium meliloti* glycanases ExoK and ExsH. *J. Bacteriol.* **180,** 4184–4191
38. Kelly, S. J., Muszyński, A., Kawaharada, Y., Hubber, A. M., Sullivan, J. T., Sandal, N., Carlson, R. W., Stougaard, J., and Ronson, C. W. (2013) Conditional requirement for exopolysaccharide in the *Mesorhizobium-Lotus* symbiosis. *Mol. Plant. Microbe Interact.* **26,** 319–329
39. Gerwig, G. J., Kamerling, J. P., and Vliegenthart, J. F. G. (1978) Determination of the D and L configuration of neutral monosaccharides by high-resolution capillary G.L.C. *Carbohydr. Res.* **62,** 349–357
40. Kawaharada, Y., Kelly, S., Nielsen, M. W., Hjuler, C. T., Gysel, K., Muszyński, A., Carlson, R. W., Thygesen, M. B., Sandal, N., Asmussen, M. H., Vinther, M., Andersen, S. U., Krusell, L., Thirup, S., Jensen, K. J., *et al.* (2015) Receptor-mediated exopolysaccharide perception controls bacterial infection. *Nature* **523,** 308–312
41. Wu, J. A., and Serianni, A. S. (1991) D-Penturonic acids: solution studies of stable-isotopically enriched compounds by ^{1}H- and ^{13}C-N.M.R. spectroscopy. *Carbohydr. Res.* **210,** 51–70
42. Lundborg, M., and Widmalm, G. (2011) Structural analysis of glycans by NMR chemical shift prediction. *Anal. Chem.* **83,** 1514–1517
43. Jansson, P.-E., Kenne, L., and Schweda, E. (1987) Nuclear magnetic resonance and conformational studies on monoacetylated methyl D-glucose- and D-galactopyranosides. *J. Chem. Soc., Perkin Trans.* **1**, 377–383
44. Amemura, A., Hisamatsu, M., Ghai, S. K., and Harada, T. (1981) Structural studies on a new polysaccharide, containing D-riburonic acid. *Carbohydr. Res.* **91,** 59–65
45. Benesi, A. J., Falzone, C. J., Banerjee, S., and Farber, G. K. (1994) NMR assignments for the Aldopentoses. *Carbohydr. Res.* **258,** 27–33
46. Hanniffy, O. M., Shashkov, A. S., Moran, A. P., Prendergast, M. M., Senchenkova, S. N., Knirel, Y. A., and Savage, A. V. (1999) Chemical structure of a polysaccharide from *Campylobacter jejuni* 176.83 (serotype O: 41) containing only furanose sugars. *Carbohydr. Res.* **319,** 124–132
47. Roslund, M. U., Aitio, O., Wärnå, J., Maaheimo, H., Murzin, D. Y., and Leino, R. (2008) Acyl group migration and cleavage in selectively protected β-D-galactopyranosides as studied by NMR spectroscopy and kinetic calculations. *J. Am. Chem. Soc.* **130,** 8769–8772
48. Brecker, L., Mahut, M., Schwarz, A., and Nidetzky, B. (2009) *In situ* proton NMR study of acetyl and formyl group migration in mono-*O*-acyl D-glucose. *Magn. Reson. Chem.* **47,** 328–332
49. Gil-Serrano, A., Sanchez del Junco, A., Tejero-Mateo, P., Megias, M., and Caviedes, M. A. (1990) Structure of the extracellular polysaccharide secreted by *Rhizobium leguminosarum* var. *phaseoli* CIAT 899. *Carbohydr. Res.* **204,** 103–107
50. Reuber, T. L., and Walker, G. C. (1993) Biosynthesis of succinoglycan, a symbiotically important exopolysaccharide of *Rhizobium meliloti*. *Cell* **74,** 269–280
51. Rodríguez-Navarro, D. N., Rodríguez-Carvajal, M. A., Acosta-Jurado, S., Soto, M. J., Margaret, I., Crespo-Rivas, J. C., Sanjuan, J., Temprano, F., Gil-Serrano, A., and Ruiz-Sainz, J. E., and Vinardell, J. M. (2014) Structure and biological roles of *Sinorhizobium fredii* HH103 exopolysaccharide. *PLoS ONE* 9:e115391
52. York, G. M., and Walker, G. C. (1997) The *Rhizobium meliloti* exoK gene

and prsD/prsE/exsH genes are components of independent degradative pathways which contribute to production of low-molecular-weight succinoglycan. *Mol. Microbiol.* **25,** 117–134

53. Mendis, H. C., Queiroux, C., Brewer, T. E., Davis, O. M., Washburn, B. K., and Jones, K. M. (2013) The succinoglycan endoglycanase encoded by exoK is required for efficient symbiosis of *Sinorhizobium meliloti* 1021 with the host plants *Medicago truncatula* and *Medicago sativa* (Alfalfa). *Mol. Plant. Microbe Interact.* **26,** 1089–1105
54. Reuber, T. L., and Walker, G. C. (1993) The acetyl substituent of succinoglycan is not necessary for alfalfa nodule invasion by *Rhizobium meliloti* Rm1021. *J. Bacteriol.* **175,** 3653–3655
55. Sutherland, I. W. (2001) Microbial polysaccharides from Gram-negative bacteria. *Int. Dairy J.* **11,** 663–674
56. Tielen, P., Strathmann, M., Jaeger, K. E., Flemming, H. C., and Wingender, J. (2005) Alginate acetylation influences initial surface colonization by mucoid *Pseudomonas aeruginosa. Microbiol. Res.* **160,** 165–176
57. York, W. S., Darvill, A. G., McNeil, M., Stevenson, T. T., and Albersheim, P. (1985) Isolation and characterization of plant cell walls and cell wall components. *Methods Enzymol.* **118,** 3–40
58. Gerwig, G. J., Kamerling, J. P., and Vliegenthart, J. F. G. (1979) Determination of the absolute configuration of monosaccharides in complex carbohydrates by capillary G.L.C. *Carbohydr. Res.* **77,** 1–7